AD

TECHNICAL REPORT ECOM 0423-3

FLOW FIELD WITHIN AND ABOVE A FOREST CANOPY

TASK I: STUDY OF AIRFLOW IN SIMULATED TEMPERATE AND TROPICAL FOREST CANOPIES

FORT HUACHUCA

by

W. Z. SADEH, J. E. CERMAK
and
T. KAWATANI

JULY 1969

DISTRIBUTION OF THIS DOCUMENT IS UNLIMITED

ECOM
UNITED STATES ARMY ELECTRONICS COMMAND
FORT MONMOUTH, N. J.
CONTRACT DAAB07-68-C-0423
FLUID DYNAMICS AND DIFFUSION LABORATORY
FLUID MECHANICS PROGRAM
COLLEGE OF ENGINEERING
COLORADO STATE UNIVERSITY
FORT COLLINS, COLORADO 80521

DISCLAIMER

THE CITATION OF TRADE NAMES AND NAMES OF MANUFACTURERS IN THIS REPORT IS NOT TO BE CONSTRUED AS OFFICIAL GOVERNMENT INDORSEMENT OR APPROVAL OF COMMERCIAL PRODUCTS OR SERVICES REFERENCED HEREIN.

Technical Report ECOM C-0423-3

Wind Tunnel Studies and Simulations of Turbulent Shear Flows Related to Atmospheric Science and Associated Technologies

TECHNICAL REPORT

FLOW FIELD WITHIN AND ABOVE A FOREST CANOPY

TASK I: STUDY OF AIRFLOW IN SIMULATED TEMPERATE AND TROPICAL FOREST CANOPIES

FORT HUACHUCA

by

W. Z. SADEH,* J. E. CERMAK**
and
T. KAWATANI†

Fluid Dynamics and Diffusion Laboratory
Fluid Mechanics Program
College of Engineering
Colorado State University
Fort Collins, Colorado

for

ATMOSPHERIC SCIENCES LABORATORY
U. S. Army Electronics Command
Fort Monmouth, N. J.

CER69-70WZS-JEC-TK-6

* Assistant Professor of Engineering
** Professor of Engineering
† Research Assistant

ABSTRACT

The velocity and longitudinal turbulence intensity distributions inside and above a forest canopy along its center line were investigated. For this purpose a model forest canopy was used in a meteorological wind tunnel.

The results indicate that the flow may be divided into an entrance and fully developed region followed by a short adjustment distance close to canopy end. The entrance region has a decisive effect on the flow characteristics through the canopy. The velocity and turbulence inside the canopy are strongly affected by its structure. A similar qualitative variation for both velocity and turbulence was found in and above the canopy. Its influence stretches over more than 4 roughness heights above it. Generally, the results are in relatively reasonable agreement with field measurements.

Investigation of the modified logarithmic law for describing the velocity profile above the canopy revealed that both flow parameters, i.e., friction velocity and roughness length, are not local constants. On the contrary, they vary drastically with height. It is suspected that this is due to the fact the assumption of constant shear stress throughout the boundary layer or significant portions of it is not satisfied.

TABLE OF CONTENTS

LIST OF FIGURES

1. INTRODUCTION

Wind movement within and above forest and vegetative canopy is of utmost importance in analyzing the various exchange processes which occur within such a canopy. The flow field and these transport processes are strongly affected by the canopy structure. Even if the roughness is uniformly distributed it has a strong influence on the resulting turbulent flow. Furthermore, with changing flow conditions the interaction between the velocity field and the roughness may change considerably.

In the immediate vicinity of a canopy and through it the velocity is relatively small whereas large turbulence intensity may prevail. Furthermore, a rather strong three-dimensional turbulent velocity field is generated by the roughness elements.

Theoretical analysis of this flow is extremely difficult due to the complexity of the interrelation between velocity field and roughness. Hence, for obtaining a better understanding of this problem it is imperative to carry out detailed experimental studies. Field measurements are inherently difficult due to the relatively high cost involved in setting up measurement stations, the continuous weather changing conditions and the instrumentation available for performing them. On the other hand, the wind tunnel which has proved its usefulness in fluid mechanics studies provides satisfactory conditions for investigating the flow within and outside canopies. The flow conditions can be maintained unchanged over enough long time periods for performing adequate investigations. Furthermore, suitable instrumentation and measurement techniques are available.

Study of airflow in and outside a forest canopy have been initiated in the recent past at the Fluid Dynamics and Diffusion Laboratory, Colorado State University. For this purpose a model forest canopy was employed in a meteorological wind tunnel. Surveys of the mean velocity and longitudinal turbulence intensity along the canopy center line, i.e., the x-axis, were carried out inside and above the canopy. The measurements were performed at constant upstream velocity and canopy configurations and structure. The use of modified logarithmic law for describing the velocity variation with height above the canopy was investigated.

2. EXPERIMENTAL APPARATUS

The aim of the experimental program was to investigate the flow field, i.e., mean velocity distribution and turbulence characteristics, within and above a forest canopy. This was to be achieved by using a model forest canopy in an adequate wind tunnel. This flow can be considered equivalent to flow within and above relatively high roughness elements randomly distributed in a turbulent boundary layer.

The flow within the lower atmosphere, i.e., atmospheric-surface-layer, can be simulated satisfactory in suitable boundary-layer wind tunnel. An extensive discussion about simulation of atmospheric motion by wind-tunnel flows can be found in References 1 and 2. The use of simulated wind-tunnel flow for studying flow patterns caused by trees is widely employed today. Unfortunately, most of these investigations concentrated on various particular cases. As early as 1927, Tiren (3) attempted to evaluate the drag of a conifer crown. Other studies related to different specific problems using models were conducted. For instance, model investigation of windbreaks characteristics are reported in References 4, 5, 6, 7 and 8. Field and wind tunnel drag measurements of deciduous and coniferous trees reported in References 9, 10, 11 and 12 show reasonable agreement between prototype and model results. However, dynamical simulation of full-scale tree and forest was yet attempted due to the complex structure and geometry of the former. Consequently, detailed studies of the flow within and above simulated forest canopy of random configuration is of prime importance. Furthermore, field measurements are relatively difficult and inherently costly. As a result investigation of model forest canopy using the wind tunnel was

undertaken in the Fluid Dynamics and Diffusion Laboratory at Colorado State University.

Firstly, wind tunnel studies using flexible roughness elements (13) and peg elements (14) were conducted. Next, drag measurements of model trees (15) and preliminary velocity and diffusion measurements (16) employing simulated forest canopy in a wind tunnel were performed. The model trees and canopy utilized in the aforementioned two works are generally similar to the canopy model used in the present work which is described later.

The flow in wind tunnel is of different scale than the full-scale flow and, therefore, geometrical, kinematical, dynamical and thermal similarity must be achieved. The experiments reported herein were performed under thermally neutral conditions. Hence, thermal similitude can be disregarded. Next, the size of the model trees, i.e., the roughness elements, used is not related to any particular full-scale forest tree. As a result the geometrical similarity is irrelevant.

For achieving dynamic similitude the Rossby (Ro), Froude (Fr) and Reynolds (Re) number, respectively, must be the same for both the simulated and field flow [1]. Rossby number expresses the Coriolis force effects due to the system rotation. In general, it can be eliminated from the similarity requirements if the horizontal length scale of the full-scale forest is smaller than about 150 km [1]. Since the model canopy horizontal length is not related to any particular prototype forest the Rossby number condition can be neglected. Moreover, any full-scale forest used for comparison purposes should be within the aforestated horizontal scale limit.

The body forces effects caused by specific weight differences are represented by the Froude number. These forces are produced by temperature variation over relatively small vertical distances. Hence, Froude number becomes important for flow with density stratification. Our experiments were carried out at constant ambient temperature, i.e., thermally neutral conditions. Thus, the Froude number equality requirement can be discarded.

The Reynolds number which expresses the viscous forces effect imposes a relatively strong limitation on model similitude for any laminar flow. The model canopy Reynolds number will be smaller by a few order of magnitude than the prototype flow. In other words, the viscous forces would be dominant for the simulated flow. It is, further, important to notice that generally the prototype flow is turbulent. In such a case the Reynolds number equality considering the turbulent Reynolds number for the field flow can be satisfied [1]. On the other hand, for sharp-edged bodies and flow about trees the flow is practically inertially dominated. Thus, the mean flow pattern is assumed to be Reynolds-number independent. Recent experimental investigations seem to indicate that trees drag coefficient and wake characteristics are approximately independent of Reynolds number [9, 10, 11, 12, 13, 14, 15, 16]. However, in comparing turbulence characteristics between the prototype and the simulated flow considerable caution must be exercised [1].

Finally, kinematic similarity for the upstream velocity profile and boundary conditions must be satisfied. The upstream velocity should vary following the logarithmic law characteristic of the lower atmosphere.

Futhermore, for achieving similar flow conditions the model canopy has to be located within the boundary layer. The latter does simulate the atmospheric-surface-layer. Consequently, the boundary layer must be artificially thickened.

2.1 Model forest canopy

A model forest canopy 1100 cm long and 183 cm wide was used. A schematic diagram of the canopy is displayed in Fig. 2.1 which also shows the system of coordinates used and all important dimensions. The canopy base was built of 18 identical aluminum plates 0.5 cm thick. On the face of these plates holes of 0.5 cm diameter were drilled. The model trees were inserted into these holes.

Model trees made from plastic simulated-evergreen boughs were employed. A sketch of the model tree is depicted in Fig. 2.1 which also shows its dimensions. The latter was arbitrarily selected based on commercially available plastic trees. However, based on average height of real spruce trees of 20 m [17] the height-ratio scale reduction is about 1:110.

The model trees were randomly distributed such that no distinct rows were evident but within about 6 cm diagonal grid. The elements density, i.e., number of trees per unit area σ_N , was approximately 1 tree/46 cm^2. This density number is averaged over the total area of the model canopy.

It is, further, possible to represent the plastic tree by using a combination of two simple geometrical shapes. The truck can be described by a cylinder whereas the crown by a cone (see Fig. 2.1). The crown volume is about 222 times larger than the stem volume. As a result the

trunk volume can be neglected. Then, a volumetric density number is defined as the ratio of the volume occupied by the crowns to the total volume of the canopy. The latter is 18 cm height. Since about 4360 model trees were distributed along the canopy, the volumetric density number σ_V is approximately 26%.

2.2 Wind tunnel

The experimental investigation reported herein was conducted at Colorado State University, Fluid Dynamics and Diffusion Laboratory Army Meteorological Wind Tunnel [18]. This tunnel is of closed circuit type and its axial propeller is driven by a 250 hp DC motor. The propeller is capable of generating air speeds up to about 36 m/sec in a 183 x 183 cm test section. The air speed can be changed continuously by varying the pitch of propeller blades and the motor speed. The test section is 26 m long constructed from eleven identical test sections of about 2.4 m long each. It is conceived such that a turbulent boundary layer about 60 cm thick can be obtained in the last downstream section with a smooth boundary surface. The tunnel contraction ratio is 9:1. The free stream turbulence intensity at the test section entrance, i.e., downstream of the damping screens, is less than 0.1%. A schematic diagram of the wind tunnel is displayed in Fig. 2.2 which also shows the canopy, the system of coordinates used and all important dimensions.

The tunnel ceiling can be adjusted mechanically for obtaining zero pressure gradient along the test section. For this purpose eight static pressure taps located 2.44 m apart, as shown in Fig. 2.1, were employed. The removable side panels are made of glass in order to allow visualization of the flow.

The model canopy was installed along the last 11 m of the test section (see Fig. 2.2). Its leading edge was located 15 m downstream of the test section entrance. A turbulence-generator made from flexible plastic strips (10 cm height, 0.63 cm wide and 0.019 cm thick) were regularly spaced along the entrance test section. It extends over 3 m.

A traversing mechanism, electrically operated, was employed for moving the measurement probes (Pitot-static tube and/or hot-wire anemometer) continuously along lines parallel to the x, y and z-axis, respectively. The carriage system permitted fine control of position within 1 mm.

A photograph of the model canopy installed in the wind tunnel is given in Fig. 2.3.

3. EXPERIMENTAL TECHNIQUE AND INSTRUMENTATION

3.1 Pressure and velocity measurement

Static pressures on the ceiling of the test section were measured by means of an electronic pressure meter of capacitance type (Trans-Sonic, Equibar Type 120A). This meter is a differential micromanometer with a resolution of 0.0001 mm Hg. Its overall range is 30 mm Hg and is divided in eight ranges from 0.01 to 30 mm Hg full scale.

A Pitot-static tube located 1 m upstream of the canopy and 1 m above the tunnel floor was used to measure the pressure and the free-stream mean velocity (see Fig. 2.2). A hemispherical standard Pitot-static tube with an impact orifice of 1/8-in in diameter was utilized [19]. The reading of the Pitot-static probe were also monitored by means of a Trans-Sonic pressure meter.

3.2 Mean velocity and turbulence intensity measurement

The mean velocity distribution and the longitudinal turbulence intensity within and above the roughness was measured by means of a single hot-wire anemometer. The hot-wire anemometer is the principal tool for turbulent research today. It has its widest application in turbulence measurements but it is also a very useful instrument for the measurement of mean velocity, i.e., time-averaged velocity.

In our work we were concerned with generally low velocities, ranging up to about 6 m/sec, and turbulence intensities which were low (above the canopy) and quite high (within the canopy and in its immediate neighborhood). The hot-wire system used in the present experiment is a

unit designed and built at Fluid Dynamics and Diffusion Laboratory. This is a fully transistorized hot-wire anemometer bridge of constant temperature (CT) type [20].

An examination of some previously published data on heat transfer from fine heated wire shows that there are relatively large inconsistencies among the results of different experiments [21]. Nonetheless, the general trend of the results is the same. All show clearly a power law dependence of the heat loss on wire Reynolds number. The exponent varies from 0.45 to 0.52, depending on the mean velocity, but the general tendency is to accept a square-root law, i.e., the so-called King's law [22].

In our work we always relied on an appropriate calibration curve for each particular wire used. With regard to the power law dependence, the 1/2 power law, as will be shown later, was satisfied approximately for most of the velocities of interest. It is important to notice that at very low velocities, viz., velocities smaller than about 0.10 m/sec, the King's law is not satisfied any more [21].

The simplified and operational form of the relation for the heat transfer from a wire placed normal to the flow, i.e., the King's law, assuming, as is usually done, that the wire resistance is linearly related to its temperature [21, 23] is

$$E^2 = E_o^2 + AU^{1/2} \quad , \tag{2.1}$$

where E is the actual voltage drop across the wire, E_o the voltage drop in still air (zero velocity or shielded hot-wire) and U is the undisturbed air velocity. The constant A depends on wire configuration and properties and on air properties. Furthermore, both A and E_o depends on the chosen resistance ratio. The latter expresses the ratio

of the actual wire resistance R_w to its cold resistance R_{woc} (unheated wire in still air).

If u is the fluctuation parallel to the mean velocity $\overline{U}$, Eq. (2.1) can be written

$$(\overline{E} + e)^2 = E_o^2 + A(\overline{U} + u)^{1/2} \quad , \tag{2.2}$$

where the overbar denotes mean (or time-averaged) values, and E_o is a constant under the chosen operating conditions. In the above relationship the mean velocity is designated by $\overline{U}$ and $\overline{E}$ stands for the time-averaged voltage drop across the wire, i.e., the DC voltage necessary to balance the bridge under steady conditions. The fluctuating component of the velocity is denoted by u and the corresponding instantaneous voltage drop by e, i.e., the instantaneous AC voltage. Under the assumption of relatively small fluctuations higher order terms in the binomial expression of $(\overline{E} + e)^2$ and $(\overline{U} + u)^{1/2}$ can be neglected. Then, after some manipulation (separation of the bridge voltage into DC and AC parts and taking root-mean-square of both voltage components), the turbulence intensity, which is commonly defined as $u_{rms}/\overline{U}$, is given by

$$\frac{u_{rms}}{\overline{U}} = \frac{4\overline{E}^2}{\overline{E}^2 - E_o^2} \frac{e_{rms}}{\overline{E}} \quad , \tag{2.3}$$

where the subscript rms denotes square-root of mean (time-averaged) square values, i.e., $\sqrt{\overline{u^2}}$ and $\sqrt{\overline{e^2}}$.

It is, futher, important to underline that Eq. (2.3) is valid when the mean velocity is relatively high in addition to the condition of small fluctuation. At low velocities, i.e., when $(\overline{E} - E_o)/E_o < 0.2$, the coefficient of the right side of Eq. (2.3) increases drastically [21].

Hence, at small velocities this relationship can not yield satisfactory and reliable results. Recently, a new hot-wire method for low velocities with large fluctuations was developed by Sadeh et al. [21]. This method requires in addition to the bridge module an adequate linearizer unit. A program for constructing a new hot-wire anemometer system has recently been completed. Currently, the performances of this new unit are checked. With the completion of the latter this new modular system will be employed during future experimental studies of the canopy flow.

As mentioned earlier the experiments reported in this work were carried out using a simple CT anemometer. Consequently, high turbulence intensity measurements, viz., larger than about 50 to 60%, at relatively low velocities are disputable. Nevertheless, the hot-wire survey was carried out for obtaining,at least,an overall picture of turbulence intensity variation.

In connection with the hot-wire anemometer unit the following auxiliary equipment was used:

(1) A digital DC voltmeter (Hewlett Packard, Model 3440A) for monitoring of various output voltages;

(2) A true root-mean-square meter, TRMS (DISA, Type 55D35) for measurement of rms values;

(3) A dual-beam oscilloscope (Textronix, Type 502A) for quick assessment of the output signal pattern, calibration and monitoring of the instantoueous AC signal.

A simplified block diagram of the equipment used is shown in Fig. 3.1

A wire of nominal diameter, dw , 0.005 mm and aspect ratio, l/dw, (l being the wire length) of 520 was used. The wire was made of copper-plated tungsten. A standard straight probe (DISA Type 55A22)was utilized.

In connection with this probe a coaxial cable is employed and, therefore, its resistance is taken into account in establishing the wire hot resistance.

Accurate calibration of the hot wire was of particular importance primarly at relatively low velocities within the roughness. The calibration was effected in the wind tunnel by changing the free-stream velocity. For this purpose the hot wire was located 1 m upstream of the canopy leading edge and 1 m above the tunnel floor, i.e., in the same plane with the Pitot-static tube. The latter was utilized for measuring the mean velocity. Unfortunately, the lowest stable velocity attainable in the tunnel is about 0.8 m/sec. For smaller velocity ranging between the latter and 0.5 m/sec the calibration was approximated by linear extrapolation. No calibration was performed for lower velocity than the former. Recently, a calibrator (Thermo-Systems, Calibrator Model 1125) was purchased. This apparatus permits accurate calibration in the velocity range 300 m/sec to about 5 mm/sec. Presently, this calibrator is being used.

A sample of the kind of calibration curves obtained using the wind tunnel is provided by Fig. 3.2. The 1/2 power relation ($E^2 \propto U^{1/2}$) was reasonably satisfied. It is relevant to notice that calibration curves do not extrapolate as straight line toward the origin. In all the cases the theoretical still air voltage, E_{oth} , obtained by linear extrapolation, was smaller than the measured voltage at zero velocity (hot-wire shielded), E_{om} . On the average E_{oth} was found to be about $0.935\ E_{om}$. This behavior is peculiar at low velocities due to free-convection effects. The reproducibility of the calibration curves was within 1 to 3%.

It is, further, important to notice that during the calibration the hot-wire was oriented just as it would be in the test run. This permits to account for free-convection effects.

4. EXPERIMENTAL RESULTS

This exploratory experimental investigation of flow inside and above the canopy had the following main purposes:

(1) To study the mean velocity evolution along the canopy.

(2) To investigate the turbulence intensity variation along the canopy.

(3) To examine the roughness effects on both mean velocity and turbulence.

(4) To determine guide lines for future work based on the results of this study.

The system of coordinates used in the presentation of the results is portrayed in Figs. 2.1 and 2.2. The origin is at the geometrical center of the canopy leading edge. As the experimental results are presented below, some pertinent discussion is interspersed wherever is deemed helpful for their proper interpretation.

4.1 Establishment of the flow

To begin with, the wind tunnel ceiling slope was adjusted for approximately zero pressure gradient along the test section. The latter was indicated by null differential pressure taken from eight equidistant pressure taps along the test section and a Pitot-static tube. It was located in the free stream as shown in Figs. 2.1 and 2.2. The pressure difference was approximated within 0.001 mm Hg.

The experiments were carried out at constant free-stream velocity of 6 m/sec. The latter, denoted by U_∞ , was measured 1 m upstream of the canopy by means of a Pitot-static tube.

Hereafter, unless mentioned otherwise, all the results are presented in dimensionless form. The dimensionless coordinates are defined by

$$\tilde{x},\tilde{y},\tilde{z} = x/h,\ y/h,\ z/h \quad , \tag{4.1}$$

where h is the canopy height, i.e., $h = 18$ cm , and the dimensionless velocity by

$$\tilde{\vec{V}} = \vec{V}/U_{\infty} \tag{4.2}$$

As mentioned earlier, the mean velocity in the atmospheric boundary layer is approximated by the logarithmic law [1]

$$\frac{U}{U_*} = \frac{1}{\kappa} \ln \frac{z}{z_o} \quad , \tag{4.3}$$

where z_o is the roughness length and κ stands for von Karman's universal constant. Usually, it is assumed to be about 0.4. In the logarithmic law U_* is the friction velocity

$$U_* = \sqrt{\tau_o/\rho} \quad , \tag{4.4}$$

where τ_o is the shear stress at the wall and ρ stands for air density. It is important to notice that this logarithmic universal velocity distribution law is based on the assumption of constant shearing stress throughout the boundary layer [24]. This wall law is widely used in describing the velocity distribution within the atmospheric surface layer. Both constants U_* and z_o depend on local conditions and upstream velocity. For given conditions they can be determined from the local measured velocity distribution.

The mean velocity profile within the atmospheric surface layer can be also described by a power law

$$U \propto z^{\alpha} \quad , \tag{4.5}$$

where α is a constant. Its value depends on the local roughness conditions. In Reference 25 a value of 0.28 is suggested for wooded area and of about 0.16 for open country region.

The upstream mean velocity (time-averaged velocity) was measured along the z-axis at 1 m upstream of the canopy, i.e., at $x = -1$ m, in plane $y = 0$. The measurements were performed by means of single hot-wire at 18 stations over a distance of 60 cm. In carrying out these measurement the hot-wire was positioned for maximum output. According to cosine law [23] the wire is most sensitive to the resultant normal velocity. It was found that the latter was aligned with the x-axis within less than 0.5° yaw or pitch angle.

The measured mean upstream velocity distribution along the z-axis is displayed in Fig. 4.1. The results were reproducible within about 3 to 5%. It was found by plotting the measured velocity on semilogarithmic paper that the logarithmic law is reasonably satisfied. For the given free-stream velocity of 6 m/sec and for the smooth area upstream of the canopy it was found that $U_* = 25$ cm/sec and $z_o = 0.0094$ cm.

Simultaneously, it was found that the mean velocity varied satisfactorily according to the power law. The value of the power α was approximated to be about 0.14. Its value is about 12% less than the value suggested for open country in Reference 25. Consequently, the upstream velocity distribution was deemed adequate for the experiment since both the wall law and the power law were found to be effective for the wind tunnel flow.

4.2 Mean velocity survey along the canopy

The mean velocity was measured at 10 locations along the model canopy over a distance of 12 m. Two stations were located 1 m upstream and downstream of the canopy leading and trailing edge, respectively. The measurements were performed by means of a single hot-wire anemometer (see Section 4.1) along the canopy center line i.e., in plane $y = 0$, along the x-axis. At each location the measurements were carried out at 17 stations over a distance of 60 cm along the z-axis, i.e., 8 stations were located inside the canopy and 9 stations above the canopy.

The measured velocity distributions at the aforementioned 10 positions are displayed in Figs. 4.1, 4.2 and 4.3, respectively. Within the canopy a relatively strong deceleration occurs over a distance of about 15 to 20 roughness heights, i.e., over about 3 to 4 m from the leading edge. This is clearly discerned by observing the evolution of the mean velocity as shown in Figs. 4.1 and 4.2. Similarly to pipe flow this region can be defined as the entrance region. Furthermore, most of the deceleration takes place within only about 5.5 roughness heights from the leading edge. Beyond this distance the entrance region effect is less pronounced. Nevertheless, the diminishing of the velocity is still observed up to about 20 h from the leading edge.

Subsequently, the velocity reaches a state of relative equilibrium over the remainder of the canopy. No more drastic changes do occur and a fully developed flow region is achieved. Toward the trailing edge of the canopy a slight growth is observed over a distance of about 5 h followed by a larger increase downstream of the canopy. This is due to the velocity variation along the smooth surface leewind of the canopy.

It is important to remark the roughness configuration effect on the vertical velocity gradient inside the canopy. Generally, higher velocities were measured along the trunk than along the first 1/3 of the crown. The former extends over 0.28 h whereas the latter over 0.72 of canopy thickness. Throughout the beginning of the entrance region, i.e., up to $\tilde{x} = 5.58$, the largest velocities within the canopy were monitored along about 1/2 of the trunk as shown in Fig. 4.1. This region of relatively larger velocities is called the jet region. The latter is caused by the stem spacing. Downstream of this position the flow jetting is less pronounced. Within the fully developed flow domain the jetting effect gradually vanishes. The velocity is practically constant along the stem throughout the second half of this region. Only close to the trailing edge the jetting does redevelop.

A minimum velocity was monitored at all stations at approximately half of canopy height, i.e., at about 0.3 of crown height. This minimum is followed by a slight rate of increase. A maximum is reached at the canopy outer edge, i.e., at $\tilde{z} = 1$, except for the jetting region.

It is interesting to examine the changes in velocity at constant height along the canopy, in other words, to follow the velocity evolution along particular isoheights. The results for 14 isoheights within and above the canopy are portrayed in Figs. 4.4 and 4.5, respectively. The relative extents of the entrance and fully developed flow regions within the canopy are clearly distingushed. Throughout the former the velocity decreases by about 95%. Subsequently through the fully developed region the velocity is practically constant up to about $\tilde{z} = 0.7$. Its magnitude is determined by the entrance region downwind velocity. At higher elevations the velocity oscillates within this region

with a peak at about $\tilde{x} = 28$ and a minimum around $\tilde{x} = 42$ to 45. This variation is probably due to the crown shape effect. The relatively small acceleration close to the trailing edge and downstream of it is also observed. It seems that the velocity field throughout the established flow region is determined by entrance domain conditions and crown configuration.

It is, further, important to notice that the velocity variation along and above the canopy is qualitatively similar to velocity change within the roughness. This is clearly shown in Fig. 4.5. The velocity decrease characteristic to the entrance region stretches up to more than two roughness heights above the canopy but, its horizontal extent is only about 10 roughness heights. Furthermore, the rate of decrease diminishes with height, e.g., from about 80% at $\tilde{z} = 1.11$ to approximately 10% at $\tilde{z} = 3.33$. Similarly to the flow within the canopy, a so-called fully developed region can be defined. Throughout the latter the velocity varies within about 5% around the entrance region downwind velocity at each height. The slight velocity increase toward the canopy end was also observed.

Next, based on the vertical velocity distribution the boundary-layer thickness growth along the canopy was approximated. It was defined, as commonly done, as the distance from the wall where $U/U_\infty = 0.99$. The latter was computed by smooth extrapolation of the measured velocity displayed in Figs. 4.1, 4.2 and 4.3. The results are shown in Fig. 4.6. In this figure the boundary-layer thickness is made dimensionless with respect to roughness height. The boundary-layer thickness increases gradually from 4 roughness heights upstream of the canopy to more than 5.5 h close to the canopy end. The strongest growth occurs within the entrance region. Throughout the fully developed flow domain the rate of growth is rather small, e. g.,

over 66% of the canopy length it grows only by 10% whereas the growth over the entrance region is more than 30%. It is important to bear in mind that the canopy causes the development of an internal boundary layer. Consequently, the total thickness is the result of both outer and internal boundary layer. In order to obtain a better estimation of the boundary-layer thickness velocity measurements up to about 6 roughness heights above the canopy are necessary.

The mean velocity within the atmospheric shear layer above roughness is usually described by a modified logarithmic law [26, 27] similar to basic wall law as expressed by Eq. (4.3). The modified law is

$$\frac{U}{U_*} = \frac{1}{\kappa} \ln \frac{z - d}{z_o} \quad , \tag{4.6}$$

where d is the zero-plane displacement. Thus, a third parameter is introduced because of the roughness. Generally, the zero-plane displacement is a function of the free-stream velocity and local roughness conditions. It can be determined experimentally for given flow conditions in a similar manner to the evaluation of the other two parameters U_* and z_o (see Section 4.1). In Ref. 13 is suggested that the zero-plane displacement can be approximated by the canopy height, i.e., $d = h$. This result was employed throughout the present work.

In order to assess the validity of the logarithmic law the velocity variation along the z-axis was plotted on semilogarithmic paper. A sample of the velocity distribution is displayed in Fig. 4.7 at $x = 5.0$ m. Similar velocity profiles were prevalent at the other stations including the entrance region. Two zones of linear variation can be clearly

discerned. The first zone, denoted by I , extends over a distance of about 70% of canopy height while the second, designated by II, stretches over more than one roughness thickness. It is suspected that zone I indicates the extent of canopy top wake whereas zone II the thickness of the internal boundary layer. The total boundary layer thickness is given by the internal and external boundary layer. The former is caused by the roughness and does thicken the external (or natural) boundary layer. The measurements within the outer zone (II) did not extend over enough length for obtaining a better approximation of the internal and total boundary-layer thickness than suggested in Fig. 4.6. It appears that measurements up to more than 6 roughness heights are necessary.

The friction velocity and roughness length were computed at each station for both inner and outer zone. Their behavior along the $\tilde{x}$-axis are shown in Figs. 4.8 and 4.9, respectively. In these figures the friction velocity is made dimensionless with respect to U_∞ and the roughness length with respect to canopy height h . Within the outer zone the friction velocity exhibits a drastic change throughout the entrance region. It amplifies by more than 6 times over a distance of about 10 roughness heights. Its peak value occured roughly at the middle of this region. As the fully developed domain is approached it diminishes gradually. Through the latter the friction velocity is practically constant. However, it is still about 2 times larger than at the canopy leading edge. A slight increase is observed toward the roughness trailing edge. In the inner region the friction velocity reveals a slightly periodical variation with about ±15% around 0.32 throughout both regions. The roughness length exhibits a similar change as U_* in the outer zone. On the other hand, throughout the

inner zone it decreases by about 3 times along the entrance region and leading portion of the established flow domain. Along the latter it firstly augments strongly. A maximum of approximately 0.47 is reached at $\tilde{x} = 4.5$. Subsequently, it decays drastically as the trailing edge is neared. The important feature of these results is the entrance region decisive effect upon the friction velocity, i.e., on the shear stress, and roughness length. Thus, the flow similarity parameters are pracitically determined by the entrance region flow conditions.

Based on the computed values of U_* and z_o it was found that the modified logarithmic law is reasonably satisfied along the canopy. In other words, similarity velocity profiles were obtained. The results at 5 stations along the canopy, 2 within the entrance region and 3 along the fully developed flow domain, are displayed in Fig. 4.10.

As mentioned earlier, the logarithmic distribution is based on the assumption that both U_* and z_o are constant with height at a given position and for given conditions. Hence, it is interesting to find their values from the local measured velocity variation. By means of Eq. (4.6), they were computed over successive equal intervals of about 1 to 2 cm. The results for both friction velocity and roughness length at four stations are shown in Figs. 4.11 and 4.12, respectively. One station is located in the entrance region and the remainder three are in the fully developed flow domain. They are made dimensionless with respect to U_∞ and h, respectively. A rather strong change with height is observed. Within the fully developed flow domain $\tilde{U}_*$ increases by about 10 times over a distance of 2.5 canopy heights. At the station located in the entrance region the friction velocity increases continuously up to about 1.5 roughness thicknesses being followed by a monotonical decrease. The roughness length distribution reveals a similar change. For instance, in the fully developed flow region it

increases from practically zero to more than 0.25. Consequently, the validity of the logarithmic law is disputable. Fortuitously, at first glance it appears that the velocity distribution does obey it. However, the variations with height of the friction velocity and roughness length are in contradiction with the basic assumption that they are local constants. In other words, the assumption of constant shear stress [24] is not satisfied. It is possible that over relatively very small intervals the logarithmic law is effective. On the other hand, it is not applicable throughout the entire boundary layer or significant portions of it. This is clearly indicated by the results presented.

4.3 Turbulence intensity survey

Simultaneously with mean velocity measurements the longitudinal turbulence intensity based on local mean velocity

$$T_{u_x} = \frac{u_{rms}(z)}{\overline{U(z)}} \quad , \tag{4.7}$$

was monitored. Its variations along the z-axis at 8 stations along the canopy and at two stations located 1 m upstream and downstream of the canopy, respectively, are displayed in Figs. 4.13, 4.14 and 4.15. The turbulence intensity change upstream of the canopy (at $\tilde{x} = -5.55$) is shown in Fig. 4.13. At this station the turbulence diminished approximately linearly from about 18% at $\tilde{z} = 0.056$ to 4% at $\tilde{z} = 3.33$. The latter location is 2.33 roughness heights above the canopy. Note that the free-stream natural turbulence is approximately 0.1%. The turbulence does decrease as the velocity increases. The relatively large turbulence intensity of the approaching flow is clearly discerned. Over the canopy height it decayed only by 8%, viz., from 18 to 10%.

The turbulence variation along the z-axis at canopy leading edge ($\tilde{x} = 0$) is also shown in Fig. 4.13. Its change is practically similar

to the upstream turbulence. Only along roughness height slightly larger values were measured. It is equal to the upstream turbulence beginning from $\tilde{z} = 1.11$.

Within both the entrance and fully developed flow regions relatively large turbulence intensities were measured inside the canopy. Generally, a similar variation is observed at all stations along the canopy. The turbulence augments continuously along the stem and along about 3/4 of the crown. At all stations it reaches a maximum followed by a subsequent decay. It is important to notice that these local maxima were monitored at approximately the same heights at all the stations along the canopy. It was measured at $\tilde{z} = 0.83 \pm 10\%$.

Throughout the entrance region turbulence intensity as high as 90% was recorded. The latter was measured at $\tilde{x} = 16.66$. At the other two stations, i.e., at $\tilde{x} = 5.55$ and 11.11 , maxima of about 70% were monitored. As mentioned earlier, these high turbulence results are disputable due to low velocities prevailing inside the canopy and the hot-wire system employed. However, undoubtedly they do indicate the local turbulence behavior. As the canopy top is approched the turbulence decayed gradually. At this position intensities of 60 to 65% were measured. Above the roughness the turbulence attenuates monotically. Over a distance of 2.33 roughness heights it diminished to about 7 to 10%.

Within the established flow domain a similar variation was monitored. Lower levels of turbulence were measured inside the canopy. Nevertheless, maxima of 70 to 80% were still recorded. The results

are shown in Figs. 4.14 and 4.15. At canopy top slightly smaller turbulence than within the entrance region was measured. At all stations it was smaller than 60%. Above the canopy it decayed in a similar manner as through the entrance region but generally, lower values were measured.

The turbulence variation downstream of the canopy is displayed in Fig. 4.15. Lower turbulence was measured along the canopy height, however, it was still possible to discern a maximum of about 48%. The latter was measured at $\bar{z} = 0.5$. Above the canopy, starting from $z = 1.11$, it was practically equal to the turbulence within the established flow region. Thus, the influence of the roughness extended downstream of it. In order to assess the roughness effects downstream of it, measurements over larger distance are needed.

It is, further, important to examine the turbulence intensity variation along particular isoheights. Thus, to follow the turbulence evolution along the roughness inside and above as determined by its configuration. The results for 8 isoheights inside and above the canopy are shown in Figs. 4.16 and 4.17, respectively. The turbulence does increase dramatically inside the canopy through the beginning of the entrance region. Based on its value upstream of the canopy (at $x = -1$ m) the turbulence is amplified more than 7 times over a distance of about 5.5 roughness heights. It should be recalled that the velocity decreases by about 95% over this distance. Subsequently, through the remainder of the entrance region and extablished flow domain the turbulence revealed an irregular periodical variation. The oscillations are more prominent along the crown than along the stem. Thus, the roughness element shape causes local changes in the turbulence. As

the canopy trailing edge is neared a continuous decrease was monitored. Throughout this region the velocity exhibits a slight increase.

The turbulence amplification through the entrance region was also observed above the canopy. It occured more gradually extending from over 10 roughness heights at $\tilde{z} = 1.39$ to more than 25 h at $\tilde{z} = 3.33$. Furthermore, the degree of amplification is smaller than inside the canopy, e.g., at $\tilde{z} = 1.39$ the turbulence intensity is amplified to about 6 times its upstream value while at $\tilde{z} = 3.33$ to about 4 times. Within the established flow region the turbulence decayed slightly as the trailing edge is approached. With larger distances from the roughness the rate of decrease is smaller.

The important aspect of these results is the strong dependence of turbulence variation upon canopy structure. The roughness affects the turbulence above it up to more than two canopy heights. Thus, the boundary layer above the canopy is highly turbulent.

4.4 Comparison with field results

In order to assess the validity of simulating wind flow inside and above forest canopies in wind tunnel is of utmost importance to compare these results with field measurements. Unfortunately, as yet the published field results are rather scarce and questionable for conducting such a comparison. In particular, full-scale data about turbulence intensity variation is completely insufficient and unsatisfactory. This is probably due to the complexity of field measurements and the state of art of suitable instrumentation.

Recently, Shinn [28] reported results of mean wind and turbulence measurements in and above a jungle-like coastal forest about 30 m high. These measurements were performed under isothermal conditions at eight heights up to about 60 m and at 3000 m from any forest border. Thus, they were carried out within the fully developed flow region. The field results for the mean velocity and longitudinal turbulence intensity are displayed in Figs. 4.18 and 4.19, respectively. In these figures the mean wind is made dimensionless with respect to the uniform velocity and the vertical and horizontal (z and x-axes) distances with respect to the canopy height. Since no results about the uniform velocity are reported, it was approximated by extrapolation of the measured wind up to about 2 canopy heights above the forest. It was found to be 5.5 m/sec. The turbulence is generally anisotropic but only its longitudinal component is shown in Fig. 4.19. Throughout the canopy it is the predominant component and, furthermore, only it was measured during the wind tunnel experiment. The turbulence intensity results displayed in this figure are based on the local mean velocity.

Wind tunnel results within the established flow domain for both mean velocity and turbulence intensity are also shown in these figures. The latter was obtained at $\tilde{x} = 52.77$ ($x = 9.5$m) whereas the field results at $\tilde{x} = 100$, both locations being in the fully developed flow region. Recall that the mean velocity and turbulence intensity are practically constant throughout this region and that the model canopy extends over 61.11 roughness heights. Generally, the mean velocity does exhibit a similar qualitative variation. Moreover, throughout most of the canopy height the velocity is exactly the same. They begin to differ close to canopy top. At $\tilde{z} = 0.8$ the field velocity is larger than the wind tunnel

results by about 4% whereas at $\tilde{z} = 0.9$ by 18%. Above the canopy the difference increases. For instance, at $\tilde{z} = 1.5$ the former is larger than the latter by about 70%. A similar general agreement is obtained when comparing the wind tunnel results with some real forest measurements reported in References 3, 17, 29, 30, 31, and 32.

The longitudinal turbulence intensity change with height reveals also a similar behavior in both cases. The field results are slightly larger throughout the canopy but starting from about $\tilde{z} = 1.4$ they are practically equal. Note that the prototype turbulence intensity measured at $\tilde{z} = 0.31$ was not included since it was not recorded on the same tower as at the other stations. The local discrepancies in mean velocity and turbulence intensity are probably due to the relatively crude instrumentation employed during field investigations. Nonetheless, the important aspect is the reasonable general similarity of the wind tunnel and prototype forest results.

5. CONCLUSIONS

The results presented in this work indicate clearly that the flow characteristics inside and above the canopy are determined by the entrance (or transition) region. The latter extends over a distance of about 15 to 20 roughness heights. As yet field measurements within this domain are not available. However, a similar transition distance was observed in relation with the effectiveness of shelter belts [33]. The entrance region is followed by a fully developed flow domain which stretches over most of the canopy length. Throughout this region both the mean velocity and longitudinal turbulence intensity exhibit a state of relative equilibrium. A third region extending over about 5 roughness heights is observed close to the trailing edge. Through this region relatively small velocity increase occurred due to the flow adjustment to the conditions downstream of the canopy.

The velocity and turbulence intensity inside the canopy is strongly affected by the roughness elements shape. Slight velocity acceleration occurred along the trunk, i.e., the jetting effect, whereas it reaches a minimum along the crown. Simultaneously, the turbulence intensity is the highest at about 0.83 of canopy height. Intensities as high as 80 to 90% were monitored.

Outside and along the canopy the velocity and turbulence show a similar variation as within it. The three flow regions are easily discerned. The canopy affects the flow above it up to more than 4 roughness heights. A turbulent boundary layer extending roughly up to more than 4 roughness heights above the canopy was measured.

Generally, at each position the velocity appears to obey the modified logarithmic law. The friction velocity and roughness length do change strongly through the entrance region and are practically constant along the established flow domain. On the other hand, particular local computation of friction velocity and roughness length revealed that both vary drastically with height. Thus, the so-called characteristic parameters of the velocity profile are not local constants and cannot be determined using the logarithmic law. Consequently, the constant shear stress assumption and, moreover, the validity of this law are disputable, albeit, at first glance, it seems that the logarithmic distribution is reasonably satisfied.

Lastly, comparison with field measurement shows that the flow characteristics within and above vegetative canopies can be satisfactorily simulated in the meteorological wind tunnel. Thus, it is economically feasible to study the various effects of canopy characteristics on the flow field.

REFERENCES

1. Cermak, J. E., et al., "Simulation of atmospheric motion by wind tunnel flow," Fluid Dynamics and Diffusion Laboratory, Colorado State Univ., Fort Collins, Colo., TR CER66JEC-SI17 (1966).

2. McVehil, G. E., Ludwig, G. R. and Sundaram, T. R., "On the feasibility of modeling small scale atmospheric motions," Cornell Aero. Lab., Buffalo, N. Y., TR ZB-23228-P-1 (1967).

3. Tiren, L., "Einige intersuchungen ober die schaft form," Meddel. Statens Skogsforsoksantalt, Häfte 24, No. 4, 81-152 (1927).

4. Hirata, T., "Fundamental studies of the formation of cutting series on the center pressure, the drag coefficient of a tree and one effect of shelter belts," Toko Univ., Tokio, Bull. Forestry 45, 61-87 (1953).

5. Iizuka, H., "On the width of a windbreak," Bull. Forestry Exp. Sta., Meguro, Tokio, 56, 1-218 (1952).

6. Iizuka, H., "On the width of windbreak," Proc. Intern. Union of Forest Res. Org., 12th Congress, Oxford, Sect. 11 (1956).

7. Malina, F. V., "Recent developments in the dynamics of wind erosion," Trans. Amer. Geophys. Union (1941).

8. Woodruff, N. P. and Zingg, A. W., "Wind tunnel studies of fundamental problems related to windbreaks," U. S. Dept. of Agric., Soil Cons. Service, Rep. SCS-TP-112 (1952).

9. Sauer, F. M., Fons, W. L. and Arnold, K., "Experimental investigation of aerodynamic drag in tree crowns exposed to steady wind-conifers," U. S. Dept. Agric., Forest Service, Rep. Div. Forest Fire Res. (1951).

10. Lai, W., "Aerodynamic drag of several broadleaf tree species," U. S. Dept. Agric., Forest Service, Internal TR AFSWP-863 (1955).

11. Raymer, W. G., "Wind resistance of conifers," NPL, Teddington, Middlesex, England, Aero. Rep. 1008 (1962).

12. Walske, D. E. and Fraser, A. I., "Wind tunnel tests on a model forest," NPL, Teddington, Middlesex, England, 1078 (1963).

13. Plate, E. J. and Quraishi, A. A., "Modeling of velocity distributions inside and above tall crops," J. App. Meteo. 4, 3, 400-408 (1965).

14. Kawatani, T. and Meroney, R. N., "The structure of canopy flow field," Fluid Dynamics and Diffusion Laboratory, Colorado State Univ., Fort Collins, Colo., TR CER67-68TK66 (1968).

15. Hsi, G. and Nath, J. H., "Wind drag within a simulated forest canopy field," Fluid Dynamics and Diffusion Laboratory, Colorado State Univ., Fort Collins, Colo., TR CER68-69GH-JHN6 (1968).

16. Mercney, R. N., "Characteristics of wind and turbulence in and above model forests," J. App. Meteo., 7, 5, 780-788 (1968).

17. Shinn, J. H., Private communication, ASRTA, Fort Huachuca, Ariz. (1968).

18. Plate, E. J. and Cermak, J. E., "Micro-meteorological wind tunnel facility: Description and characteristics," Fluid Dynamics and Diffusion Laboratory, Colorado State Univ., Fort Collins, Colo., TR CER63EJP-JEC9.

19. Pankhurst, R. C. and Holder, D. W., Wind Tunnel Technique, (Sir Isaac Pitman & Sons, Ltd., London 1952).

20. "Operating and maintenance manual for Colorado State University hot-wire anemometer,", Fluid Dynamics and Diffusion Laboratory, Colorado State Univ., Fort Collins, Colo.. TR CER66-67VAS-CLF16 (1966).

21. Sadeh, W. Z., Sutera, S. P. and Maeder, P. F., "An investigation of vorticity amplification in stagnation flow," Div. of Eng., Brown Univ., Providence, R. I., TR AF1754/4, WT50 (1968).

22. King, L. V., "On the convection of heat from small cylinders in a stream of fluid," Phil. Trans. Roy. Soc., London, A, 214, 373-432 (1914).

23. Sandborn, V. A., "Metrology of fluid mechanics," Fluid Dynamics and Diffusion Laboratory, Colorado State University, Fort Collins, Colorado, TR CER66VAS32 (1966).

24. Schlichting, H., Boundary Layer Theory (McGraw-Hill Book Co., Inc., New York, 1960) 4th ed.

25. Davenport, A. G., "Gust loading factors," J. Struc. Div., Proceeding ASCE, ST3 (1967).

26. Rossby, C. G. and Montgomery, R. B., "The layers of frictional influence in wind and ocean currents," Mass. Inst. of Tech. and Woods Hole Ocean. Ins., Mass., Papers in Phys. Ocean. and Meteo., 3, 3 (1935).

27. Tan, H. S. and Ling, S. C., "Quasi-steady micro-meteorological atmospheric boundary layer over a wheat field," Lemon, E. R. (editor), "The energy budget at the earth's surface," Part II, U. S. Dept. of Agric., Agric. Res. Serv., Prod. RR72 (1963).

28. Shinn, J. H., "Analysis of wind data from a South Carolina coastal forest," R & DTR, ECOM-6036, U. S. Army Electronics Command, Atmos. Sci. Lab., Res. Div., Fort Huachuca, Ariz. (1969).

29. Cooper, R. W., "Wind movements in pine stands," Georgia Forest Res. Pap. 33, Georgia Forest Res. Coun. (1965).

30. Reifsnyder, W. E., "Wind profiles in a small isolated forest stands," Forest Science, 1, 4 (1955).

31. Poppendiek, H. F., "Investigation of velocity and temperature profiles in air layers within and above trees and brush," TR, Dept. of Eng., Univ. of Calif., Los Angeles (1949).

32. Fons, W. L., "Influence of forest cover on wind velocity," J. Forest., 38, 481-486 (1940).

33. Linde, J. van der,"Trees outside the forest," Forest Influences, Food and Agriculture Org., U.N., Rome (1962).

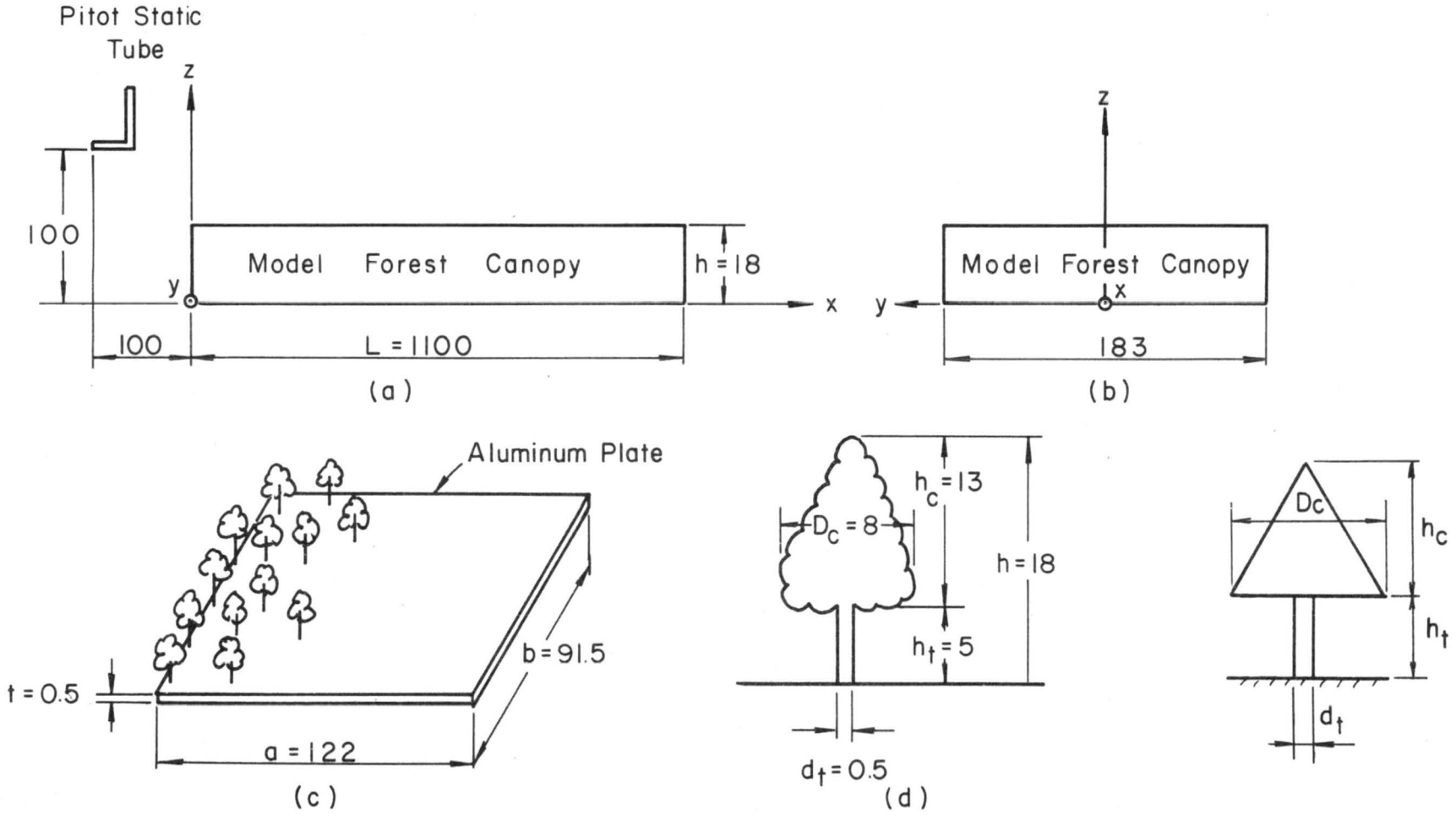

All Dimensions in Centimeters

Fig. 2.1 Sketch of Model Forest Canopy and of Model Tree.

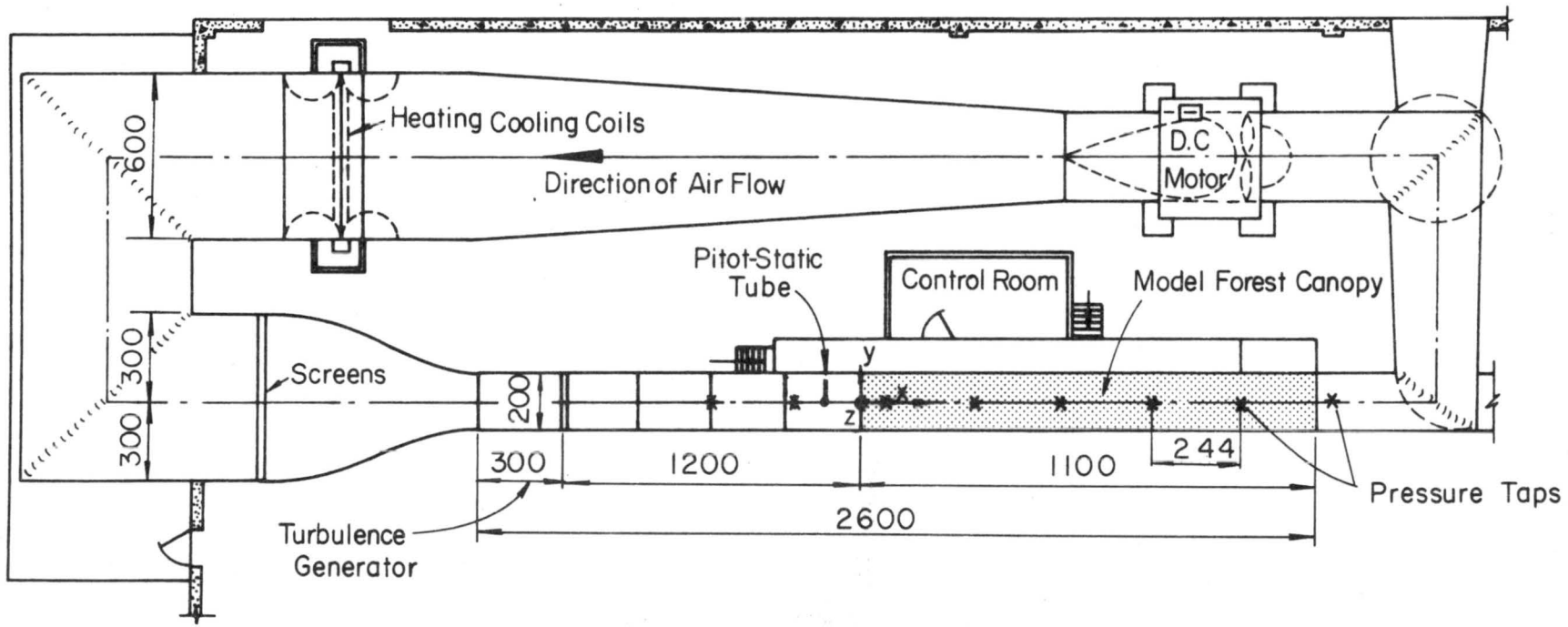

All Dimensions in Centimeters

Fig. 2. 2 Sketch of Wind Tunnel.

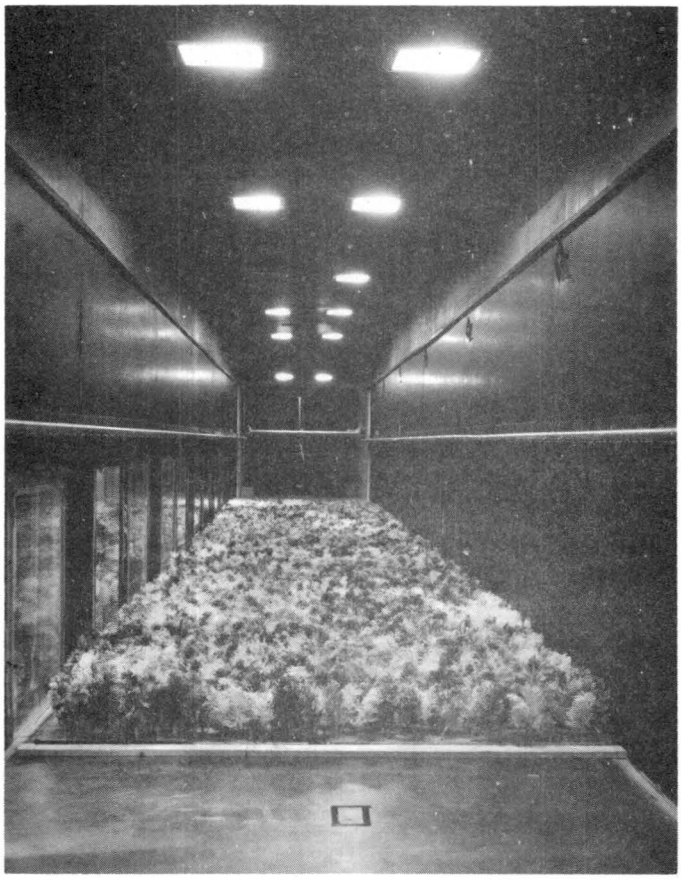

Fig. 2.3 Overall View of Model Forest Canopy and Wind Tunnel.

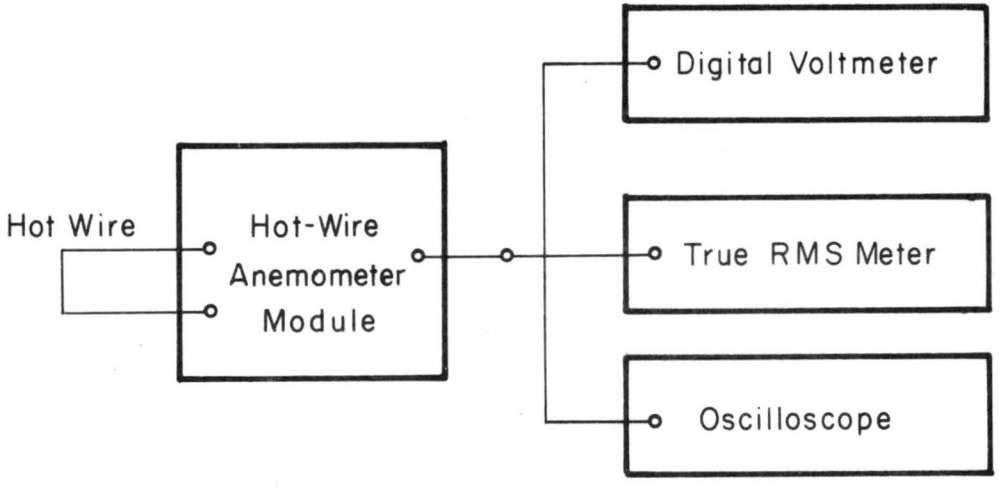

Fig. 3.1 Simplified Block Diagram of Hot - Wire Anemometer Measuring System.

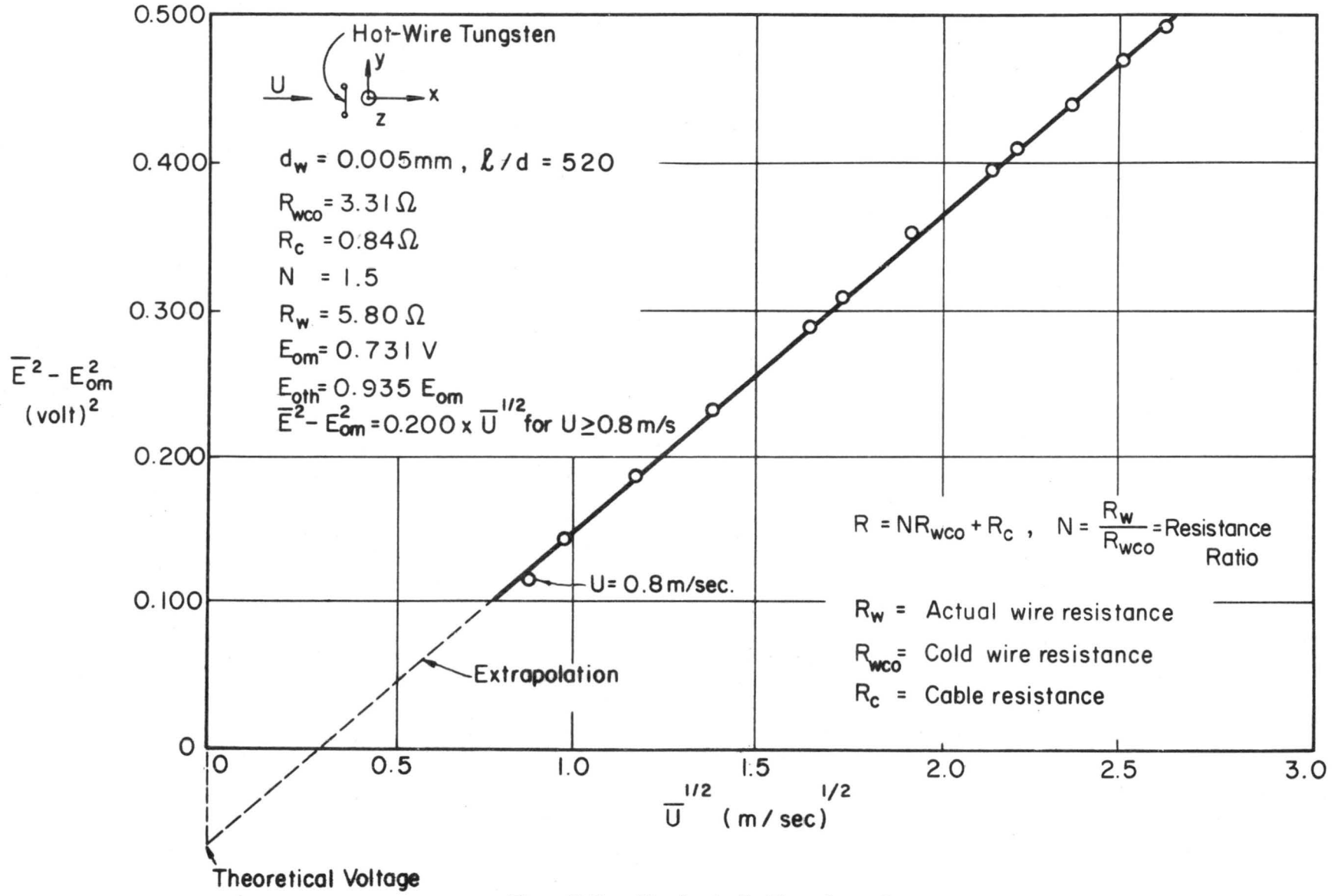

Fig. 3.2 Typical Calibration Curve.

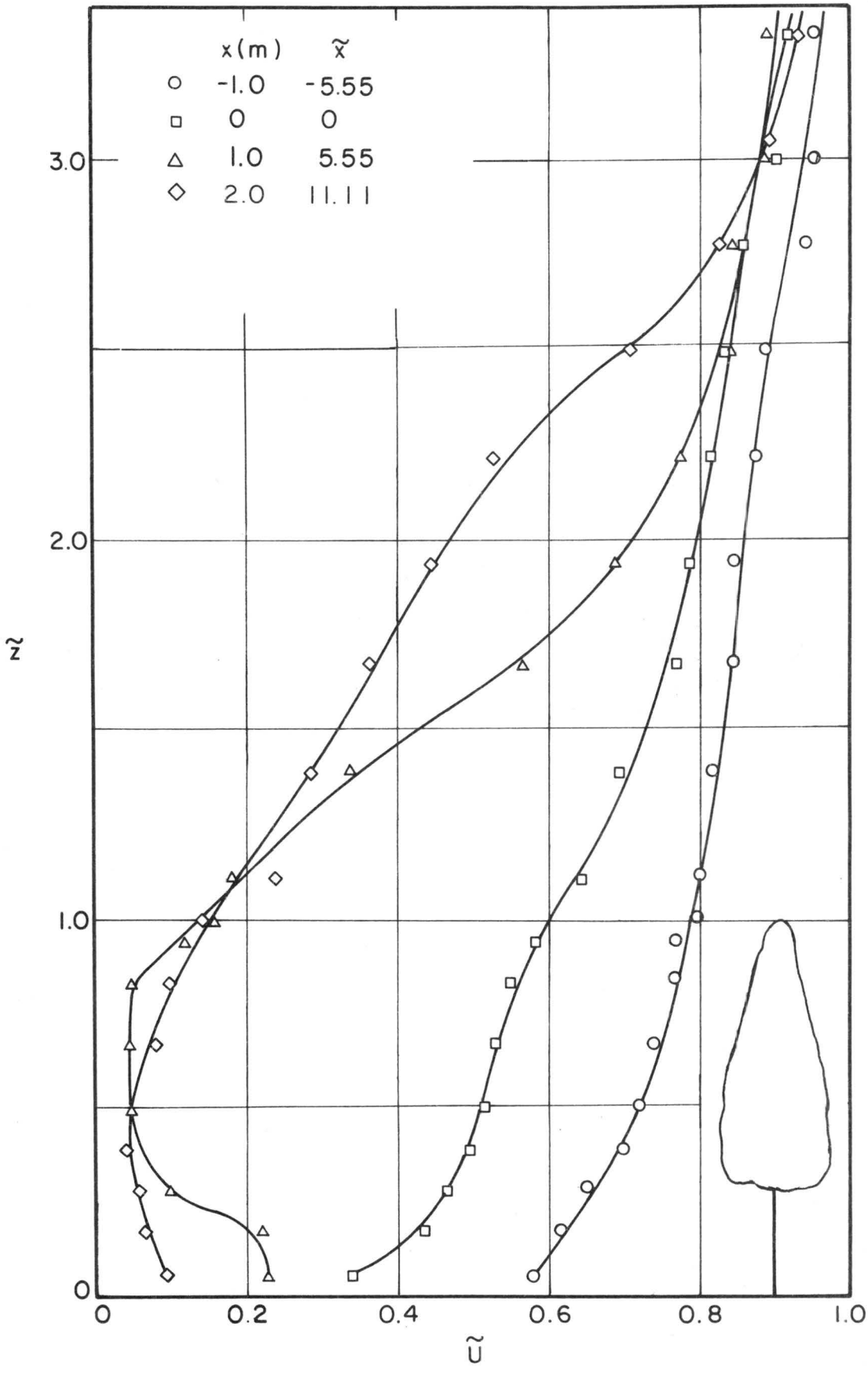

Fig. 4.1 Mean Velocity Distribution Upstream of the Canopy at $x = -5.55$, and within and above the Canopy at $\tilde{x} = 0$, 5.55 and 11.11.

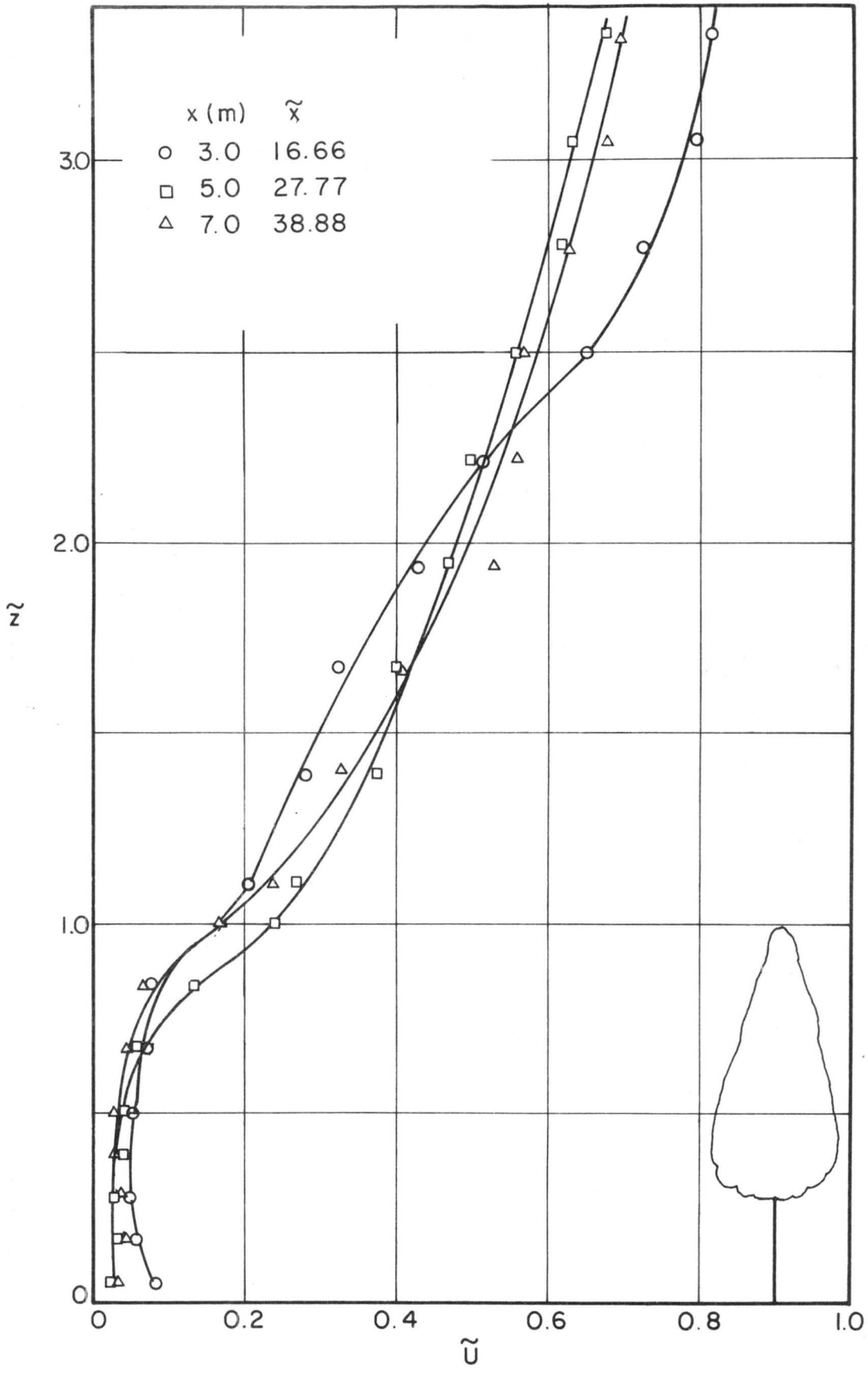

Fig. 4.2 Mean Velocity Distribution within and above the Canopy at $\tilde{x}$ = 16.66, 27.77, and 38.88.

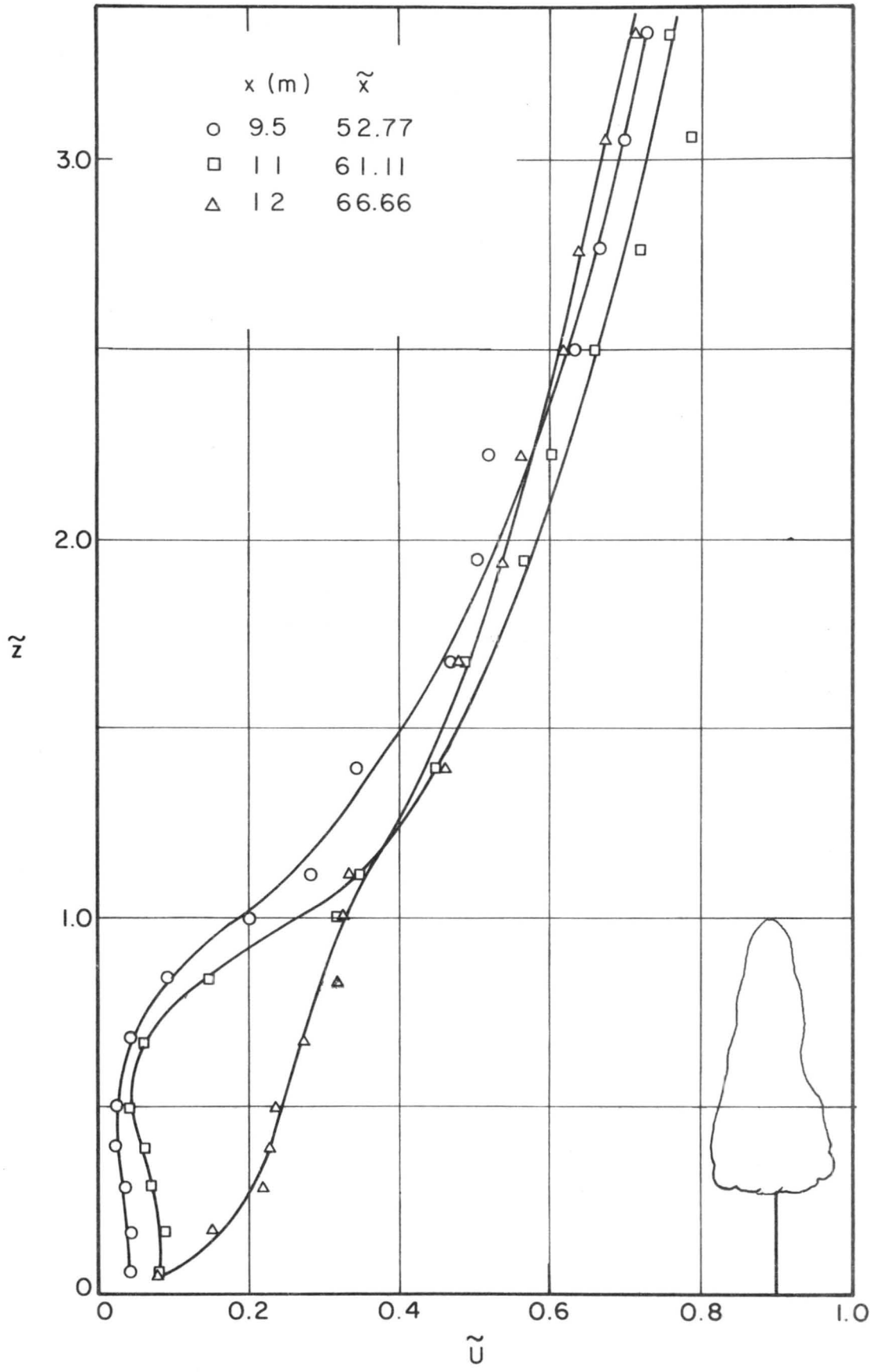

Fig. 4.3 Mean Velocity Distribution within and above the Canopy at $\tilde{x}$ = 52.77 and 61.11 and Downstream of it at $\tilde{x}$ = 66.66.

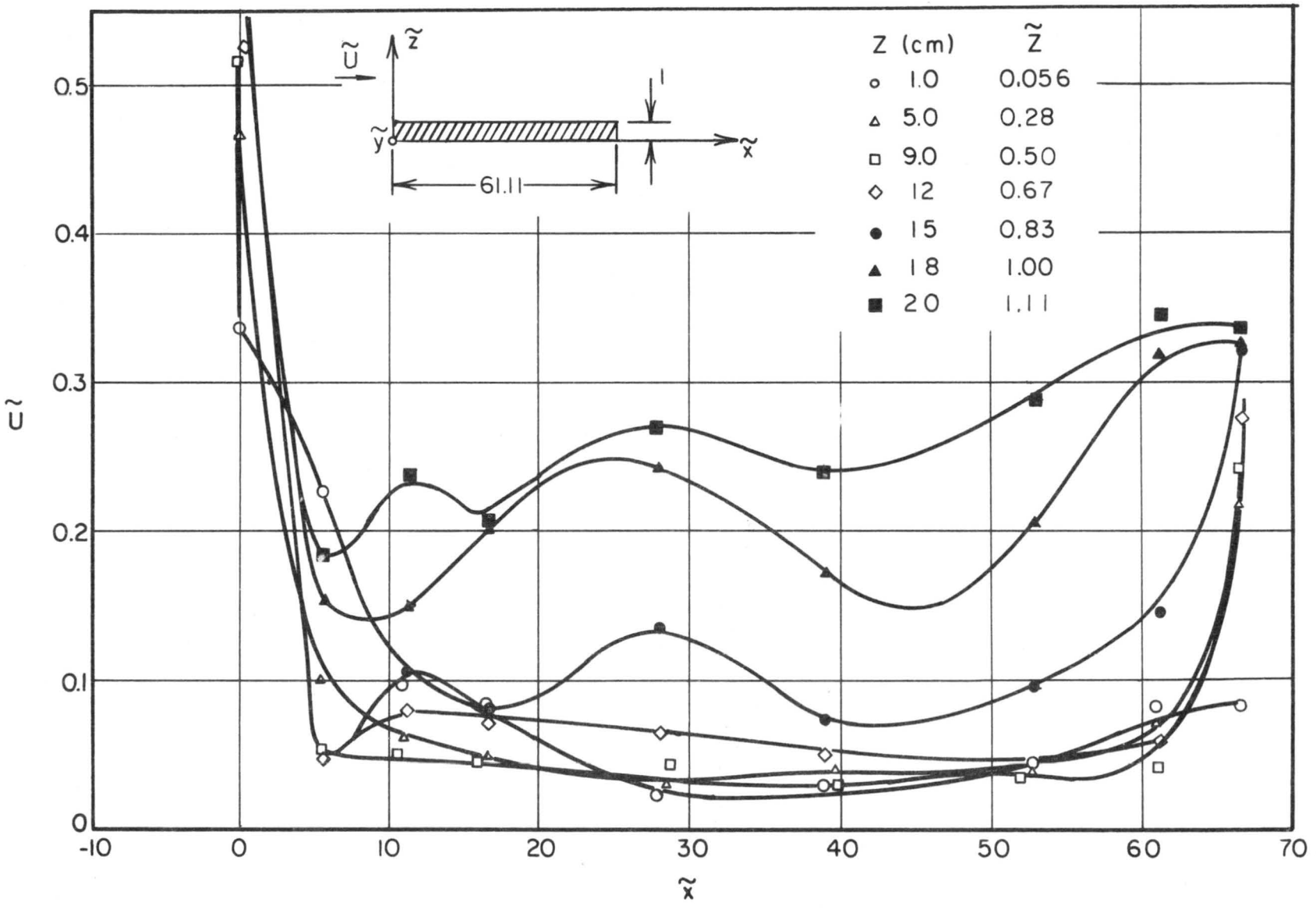

Fig. 4.4 Mean Velocity Variation along Isoheights within and at 2cm above the Canopy.

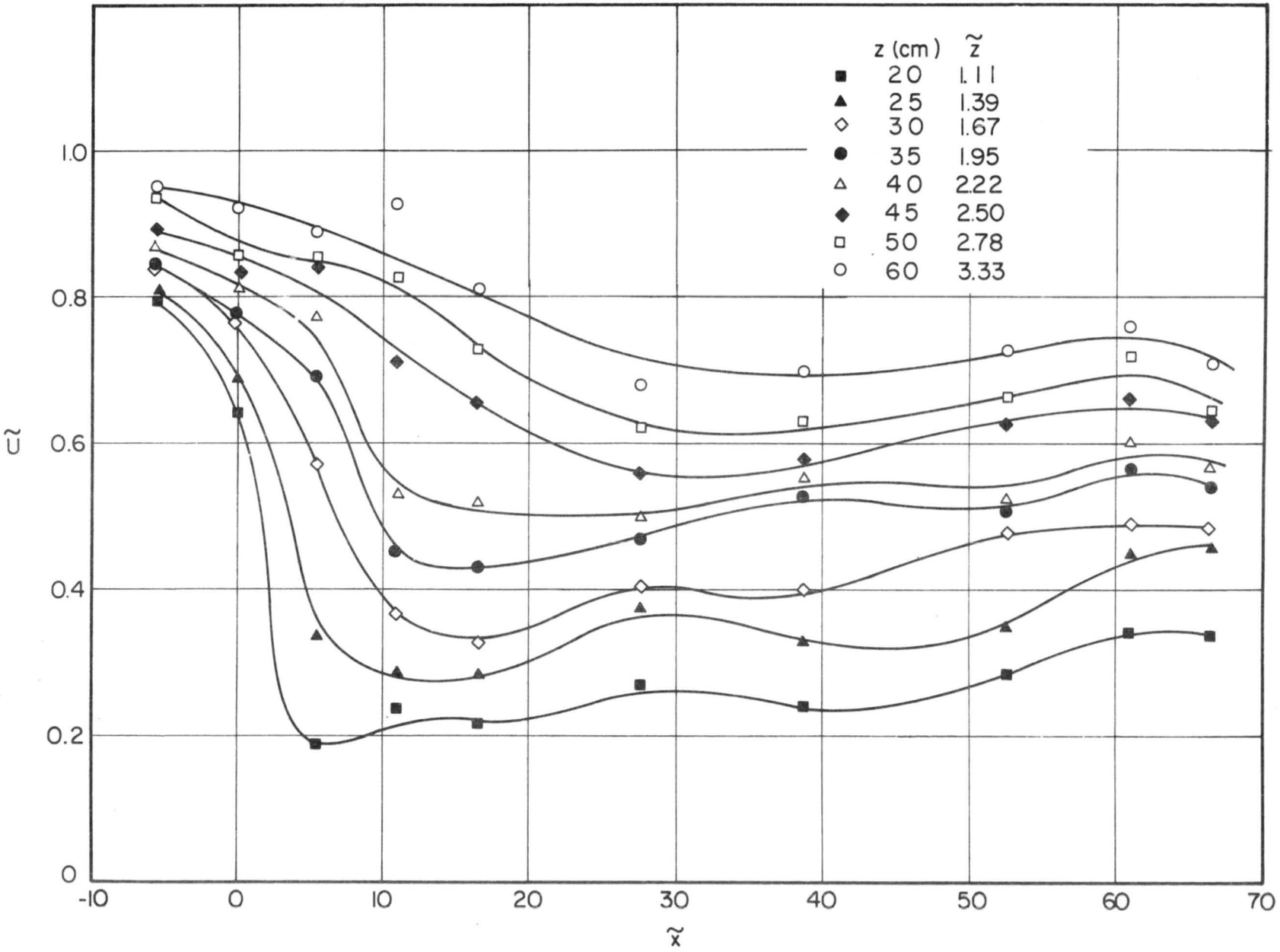

Fig. 4.5 Mean Velocity Variation along Isoheights above the Canopy.

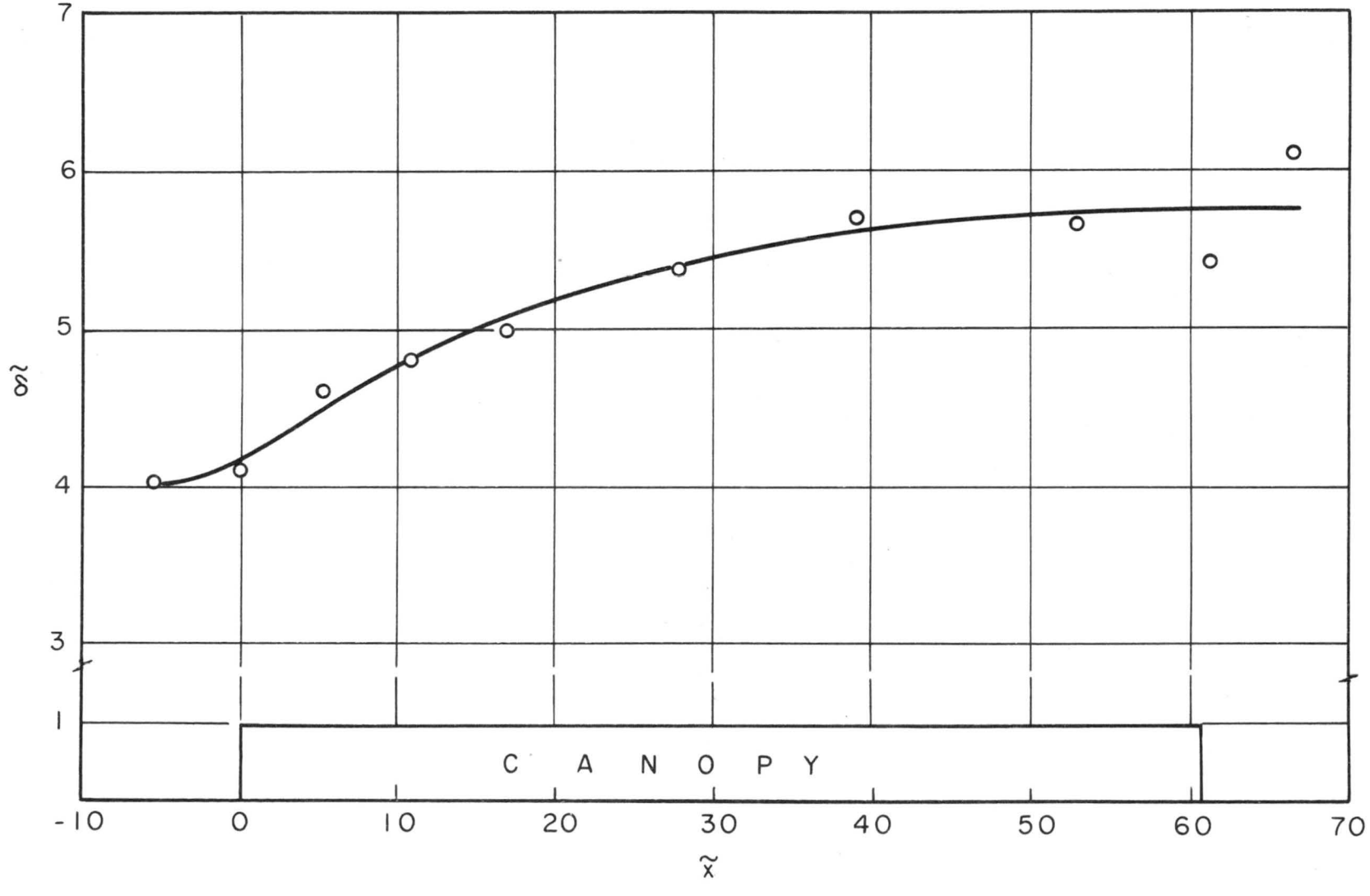

Fig. 4.6 Boundary - Layer Thickness Growth along the Canopy.

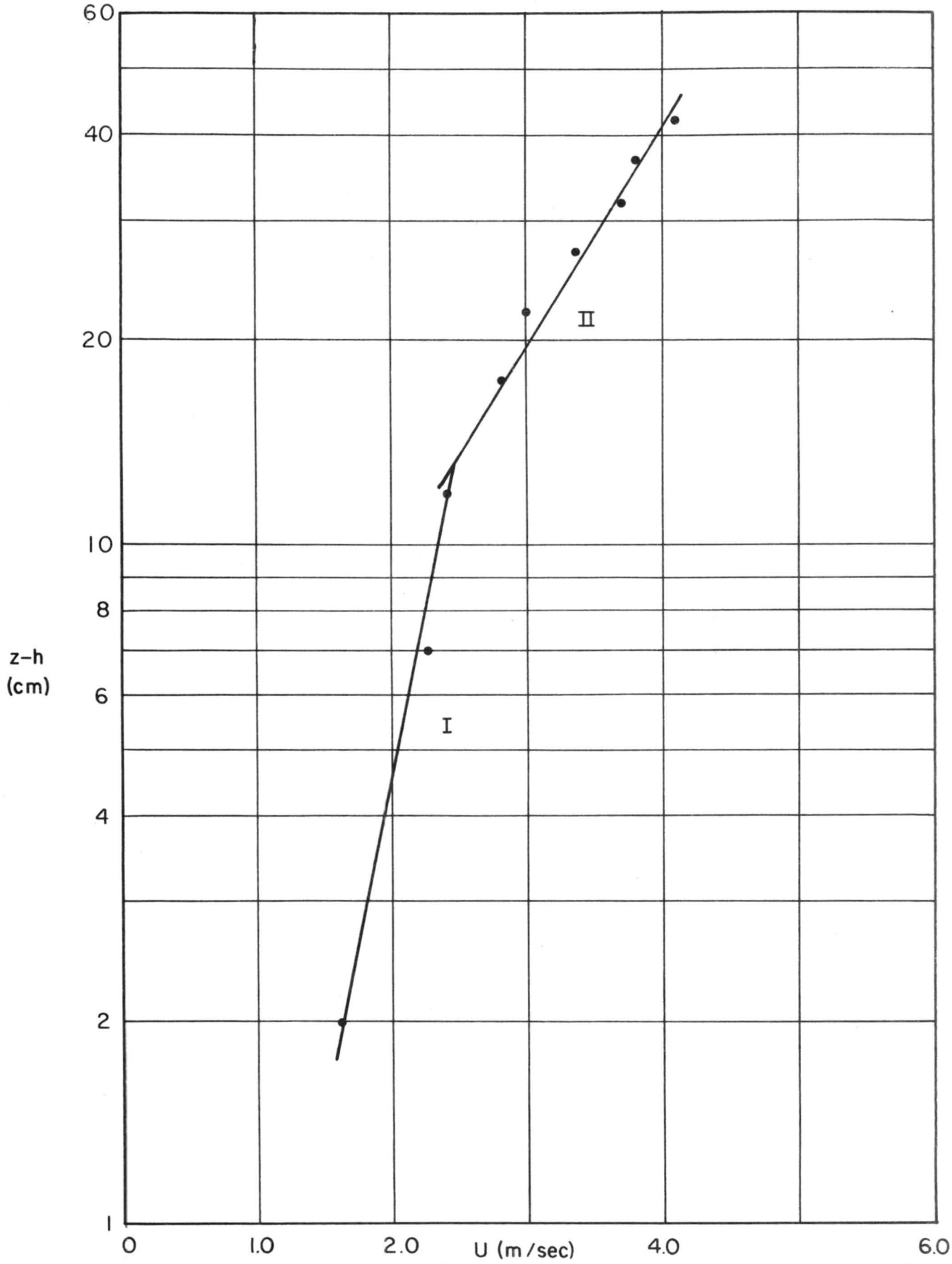

Fig. 4.7 Velocity Distribution along the z-axis above the Canopy at x=5.0m.

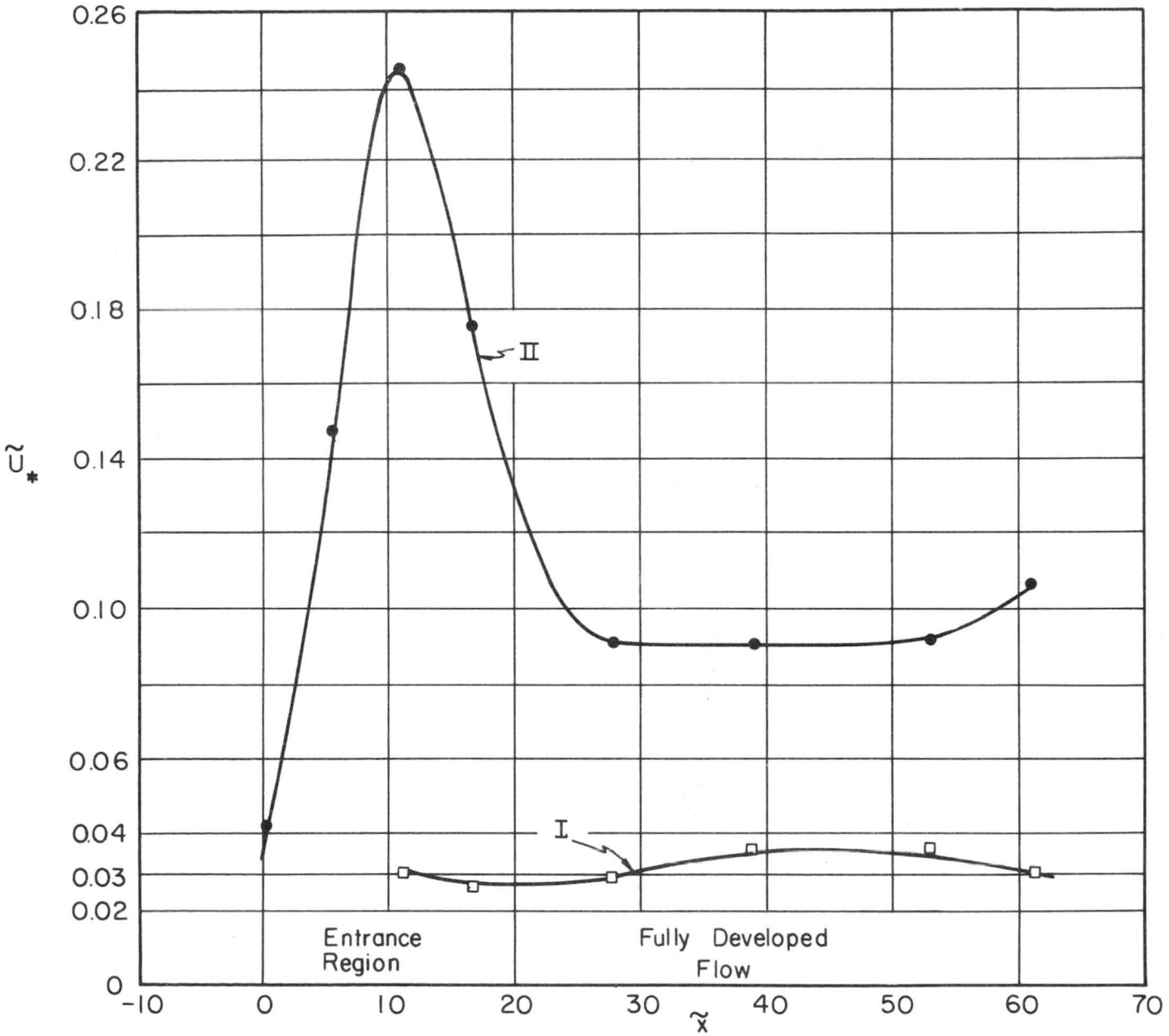

Fig. 4.8 Friction Velocity Variation along the $\tilde{x}$-axis; Inner (I) and Outer (II) Zone.

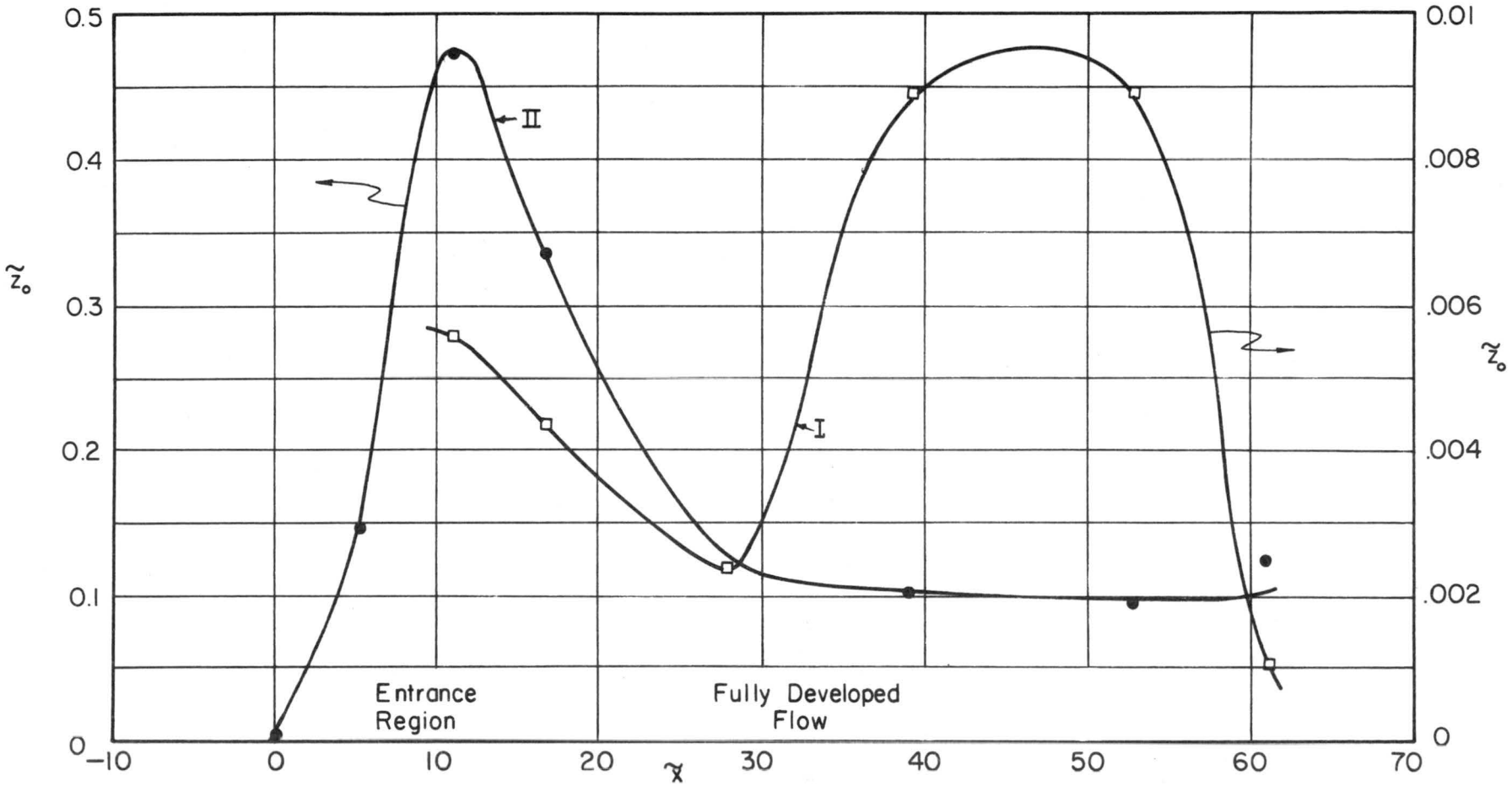

Fig.4.9 Roughness Length Variations along the $\tilde{x}$−axis; Inner (I) and Outer (II) Zone.

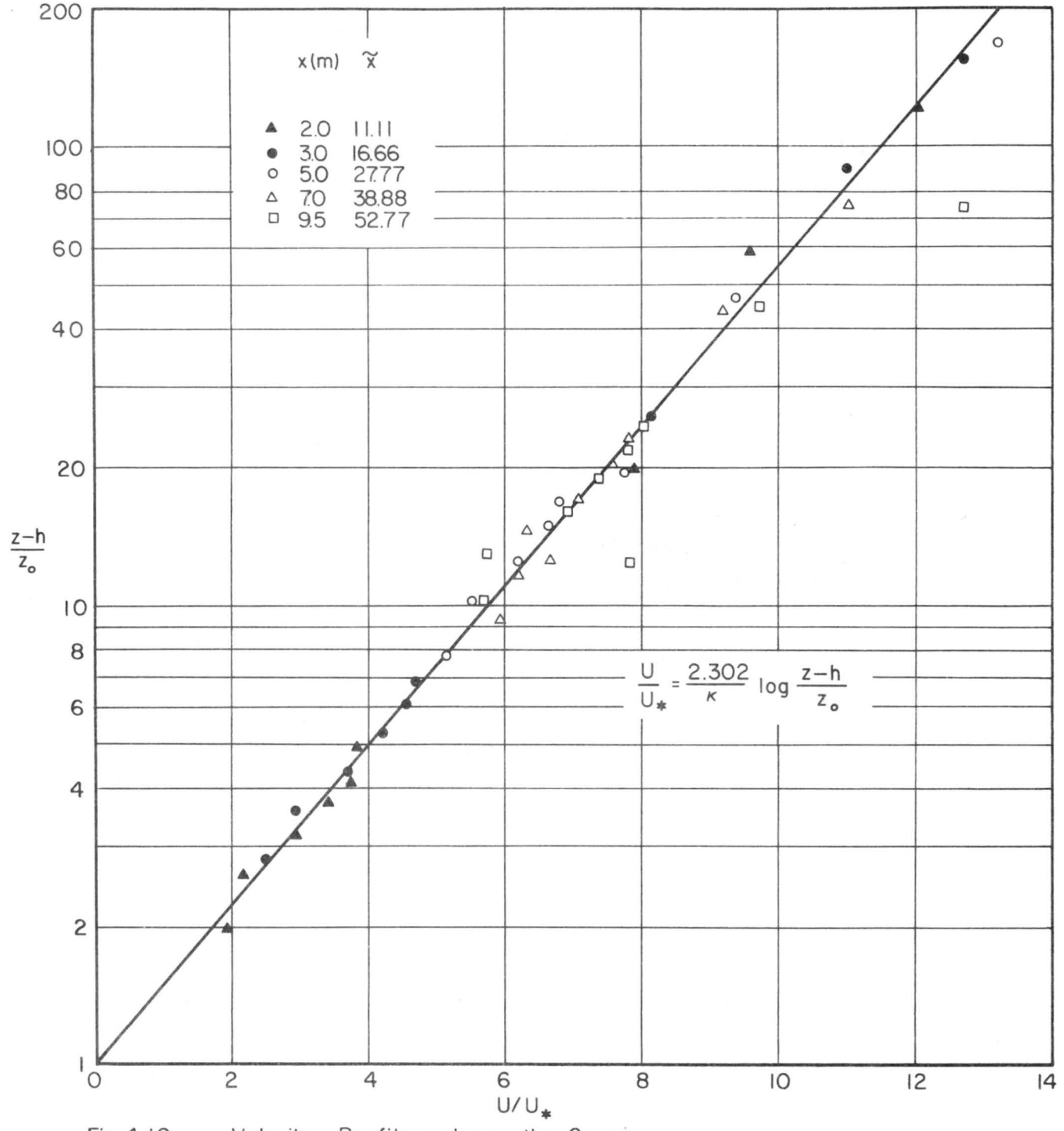

Fig. 4.10 Velocity Profiles above the Canopy.

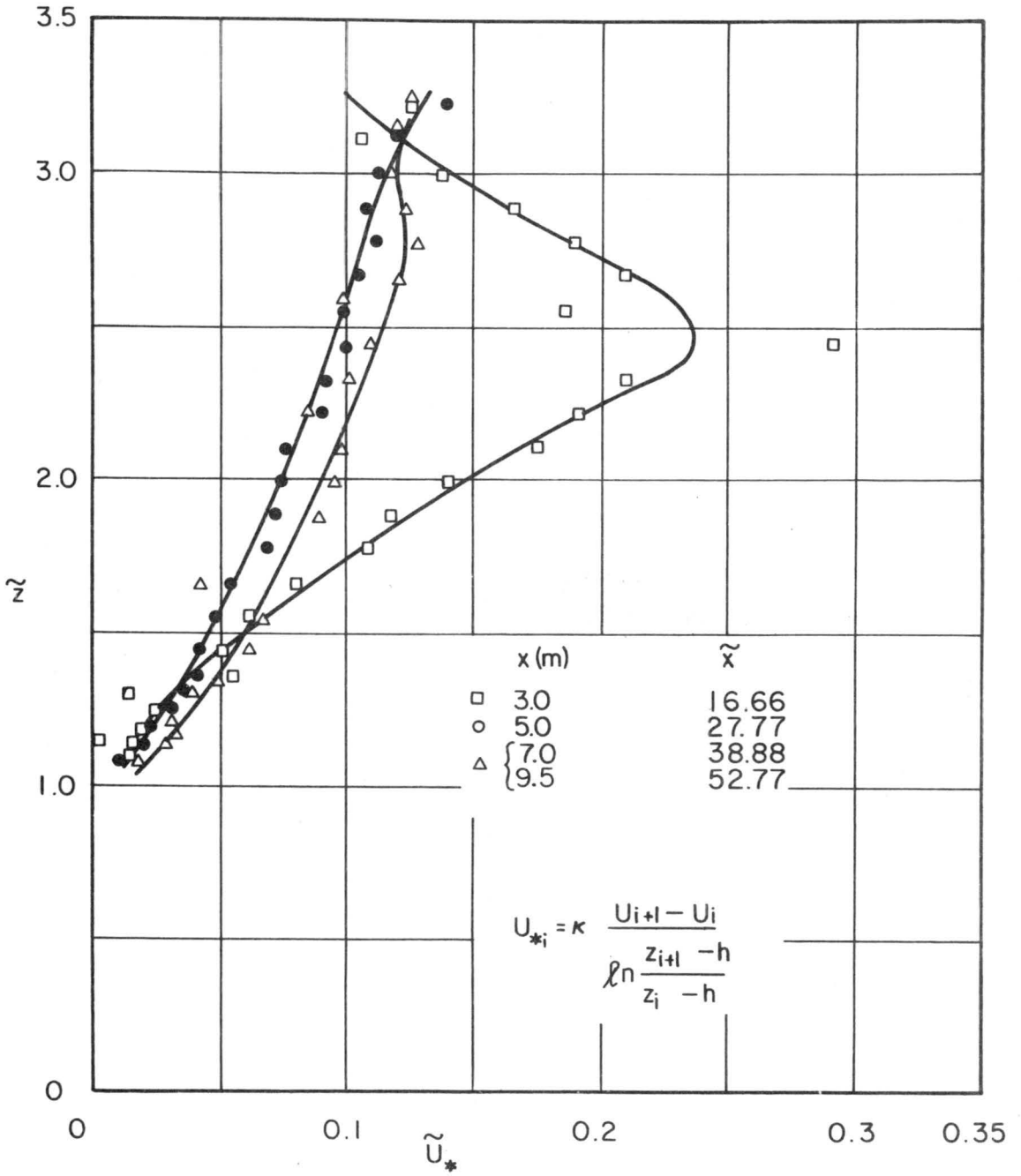

Fig. 4.11 Friction Velocity Variation with Height for given Local Conditions.

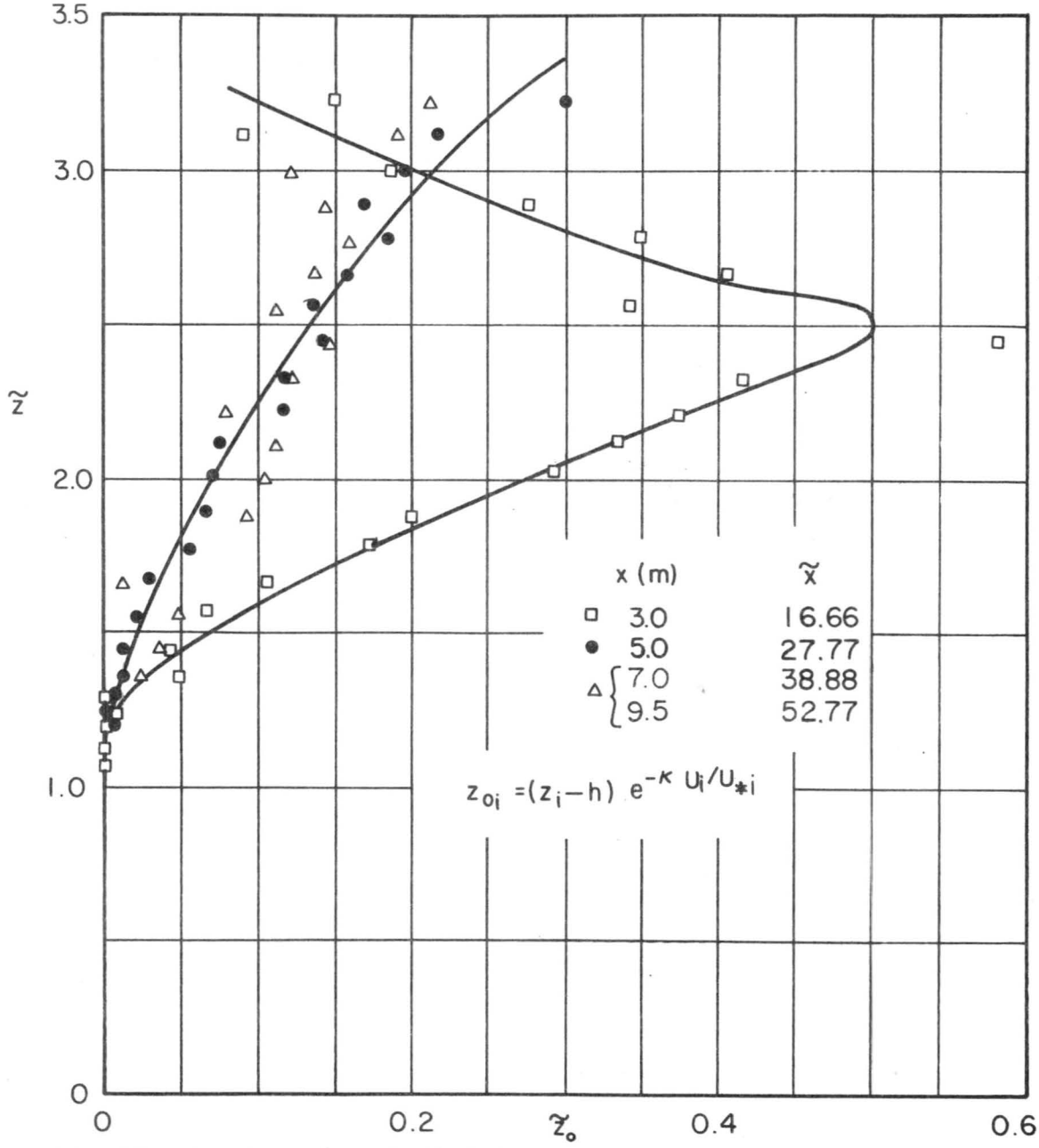

Fig. 4.12 Roughness Length Variation with Height for given Local Conditions.

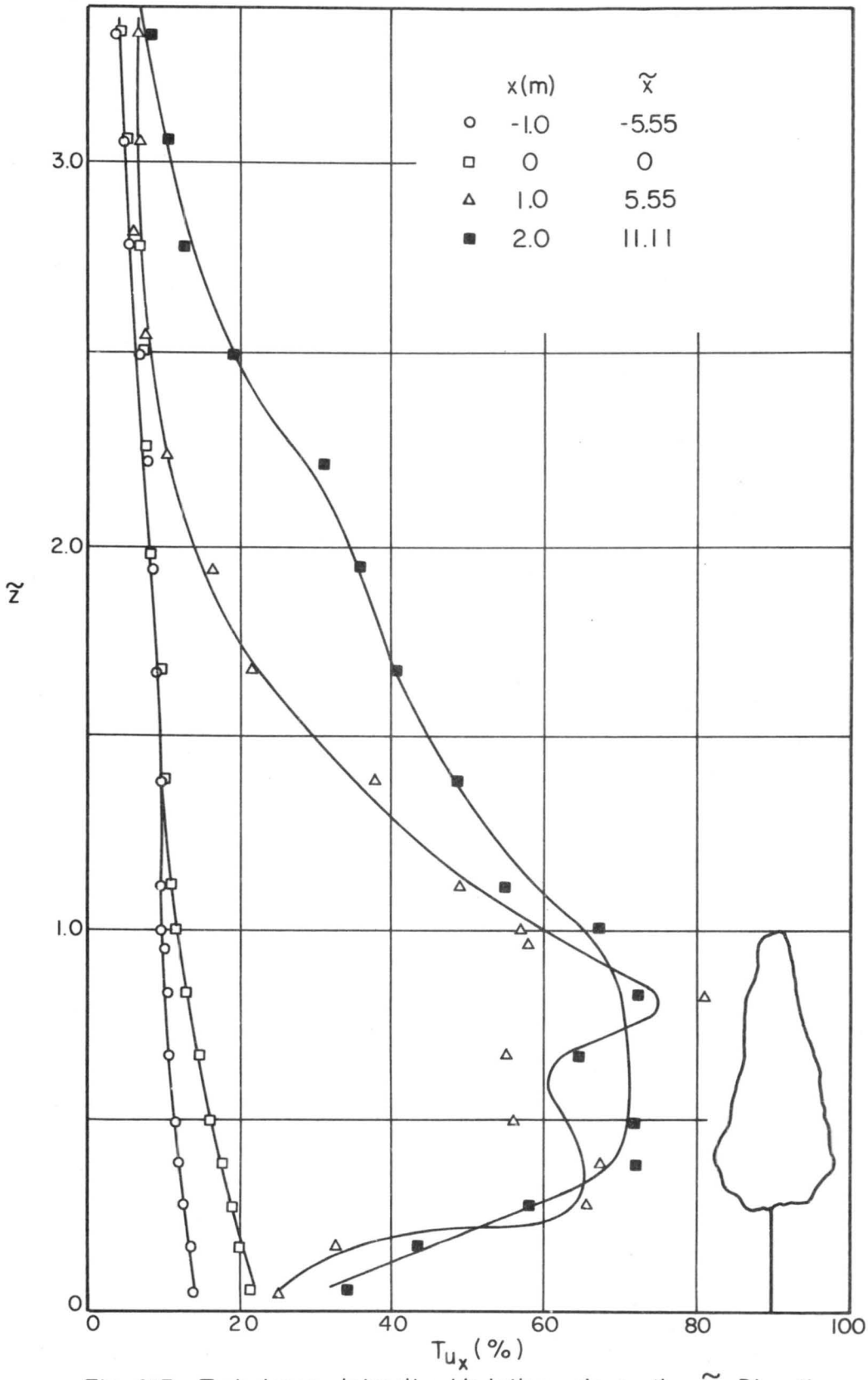

Fig. 4.13 Turbulence Intensity Variation along the $\tilde{z}$ Direction Upstream of the Canopy at $\tilde{x}$ = -5.55 and within and above the Canopy at $\tilde{x}$ = 0, 5.55, and 11.11.

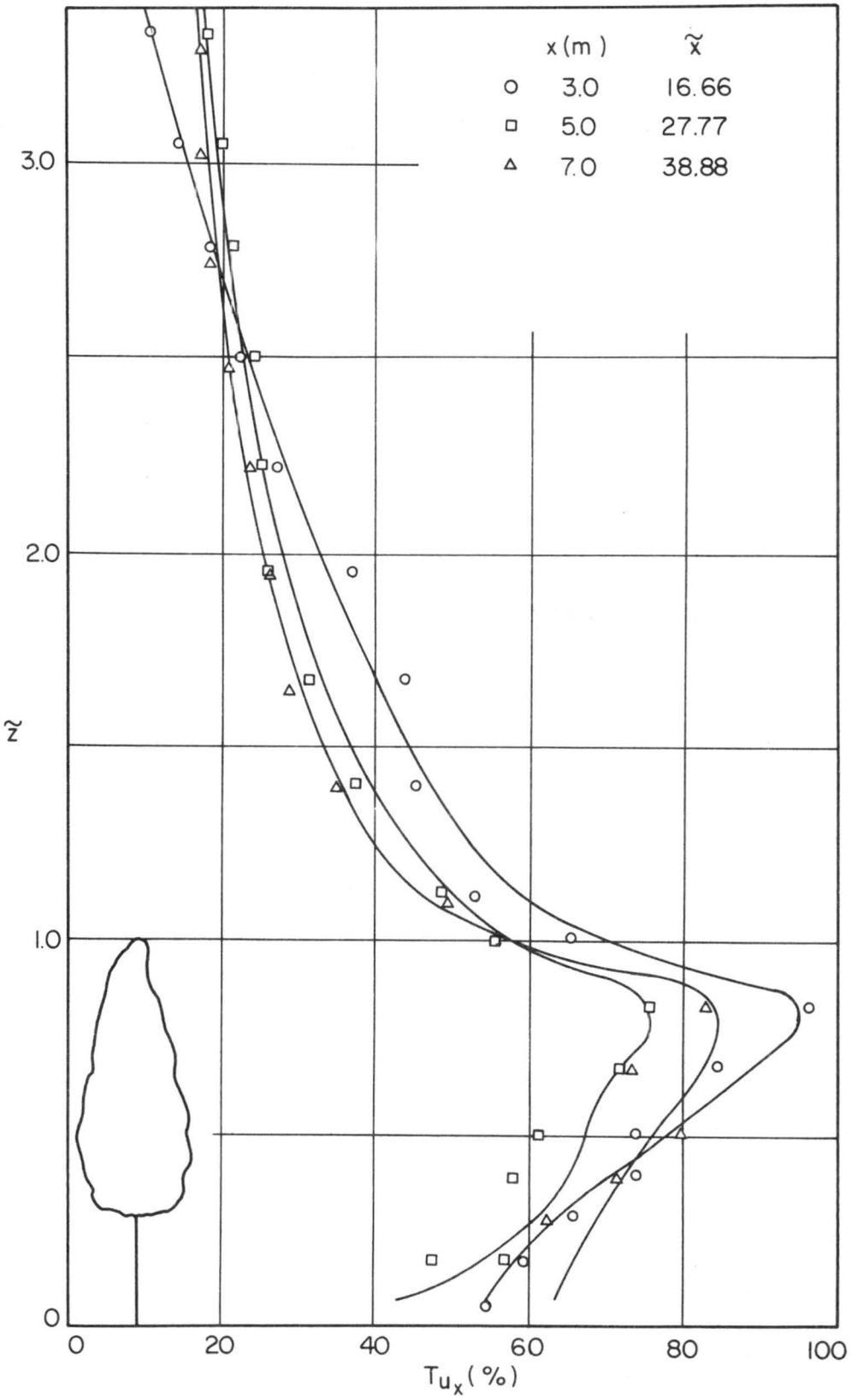

Fig. 4.14 Turbulence Intensity Variation along the $\tilde{z}$ direction within and above the Canopy at $\tilde{x}$ = 16.66, 27.77, and 38.88.

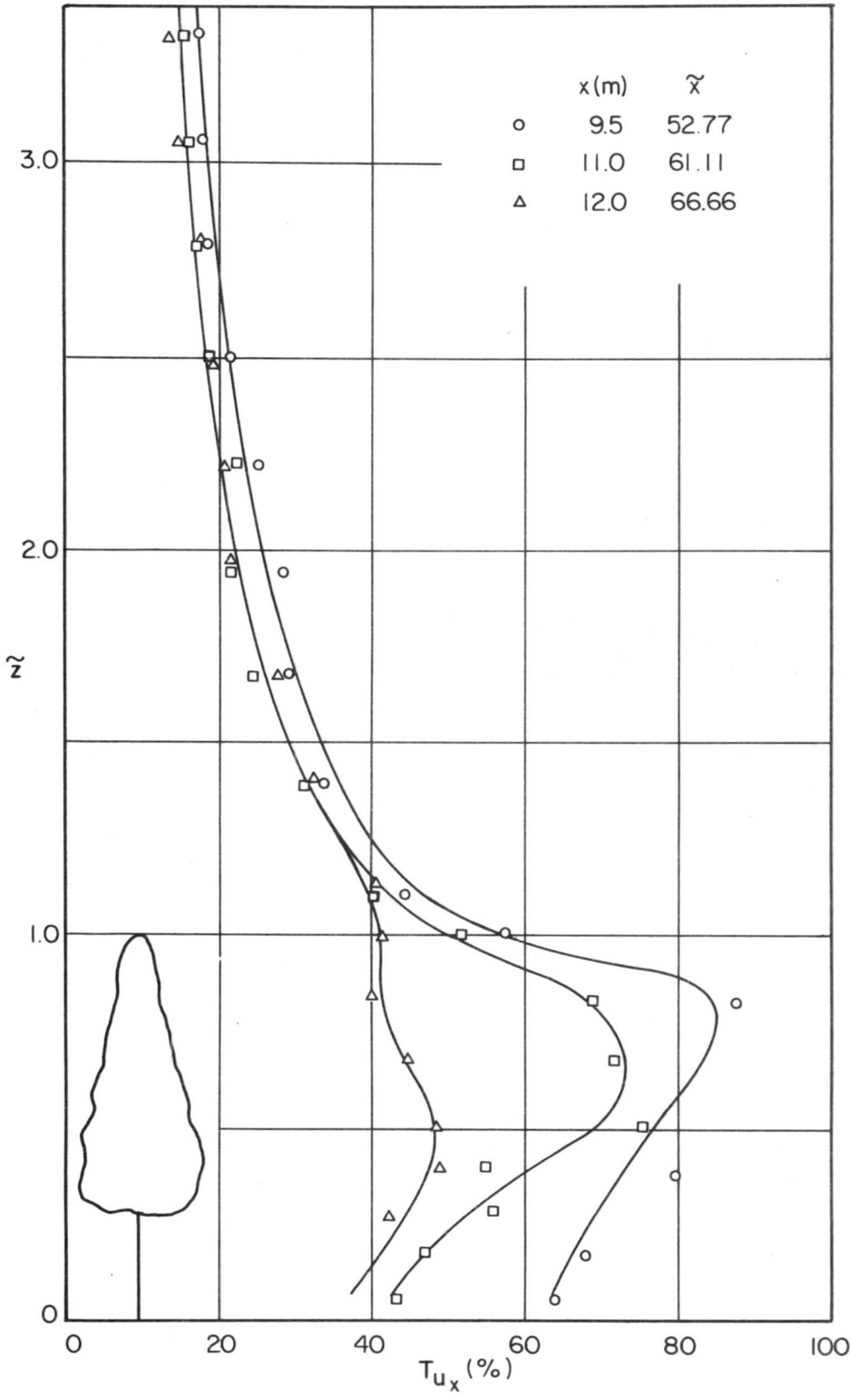

Fig. 4.15 Turbulence Intensity Variation along the $\tilde{z}$ Direction within and above the Canopy at $\tilde{x}$ = 52.77 and 61.11 and Downstream of it at $\tilde{x}$ = 66.66.

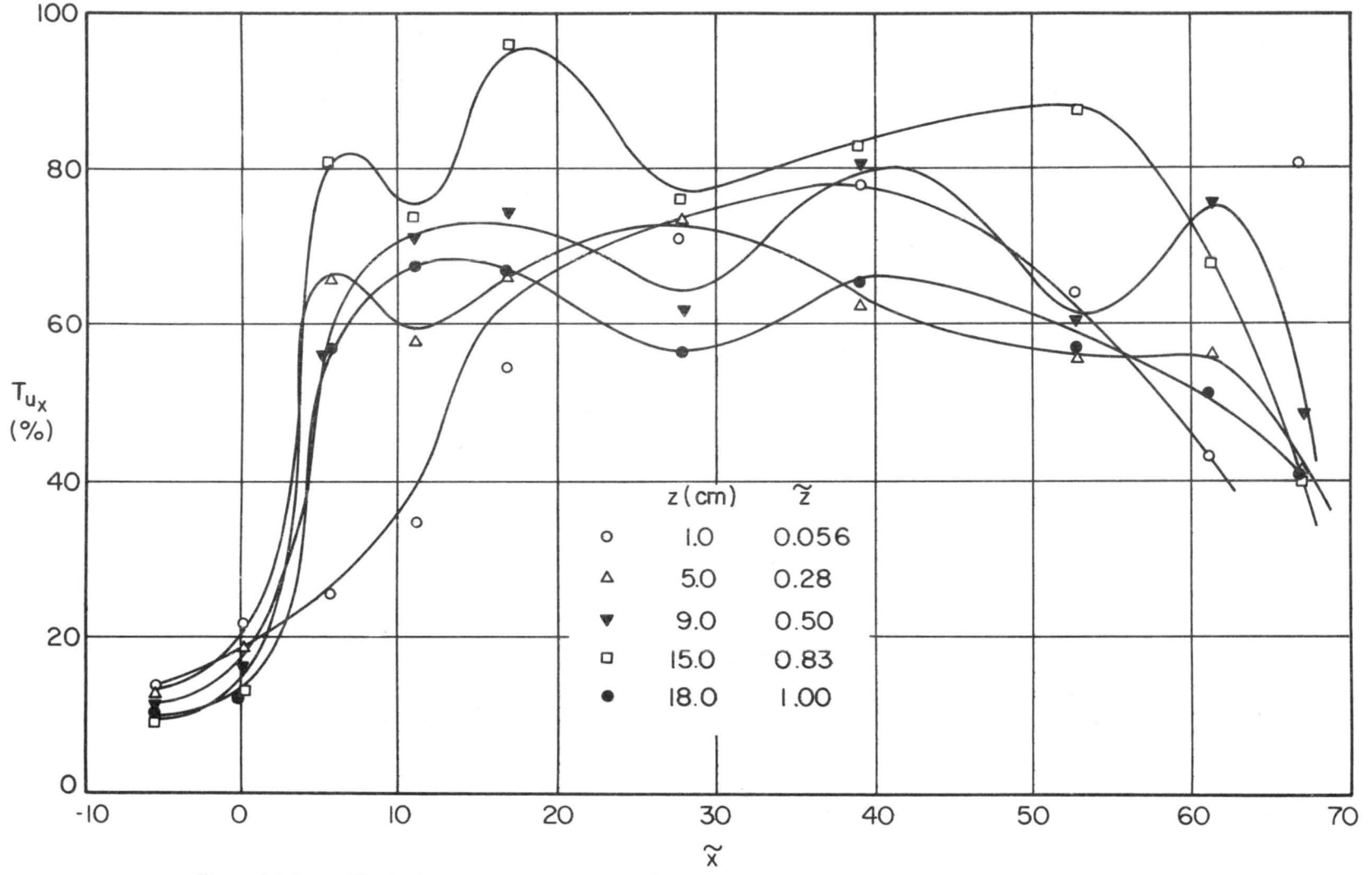

Fig. 4.16 Turbulence Intensity Change along Isoheight inside the Canopy.

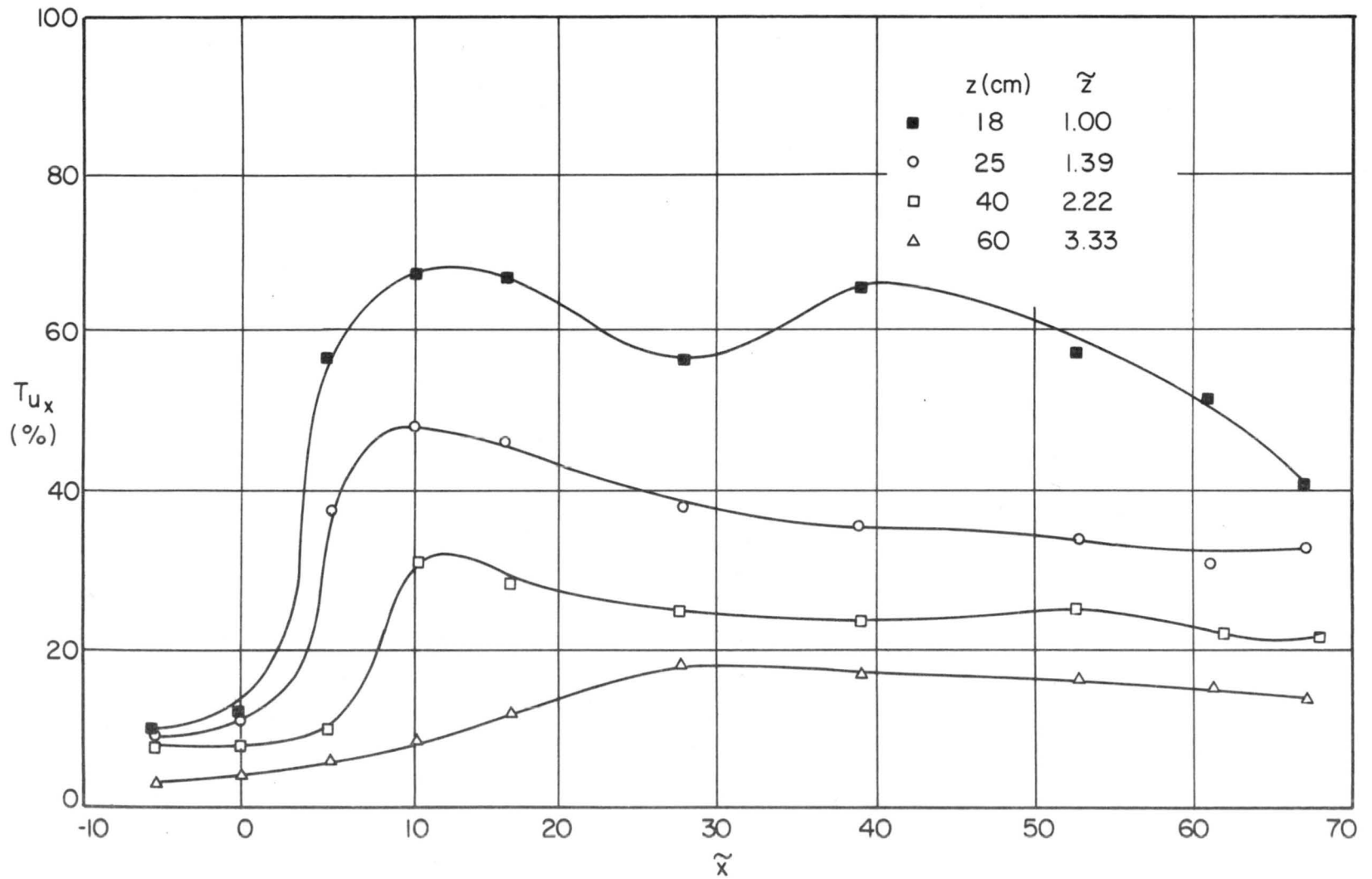

Fig. 4.17 Turbulence Intensity Change along Isoheight above the Canopy.

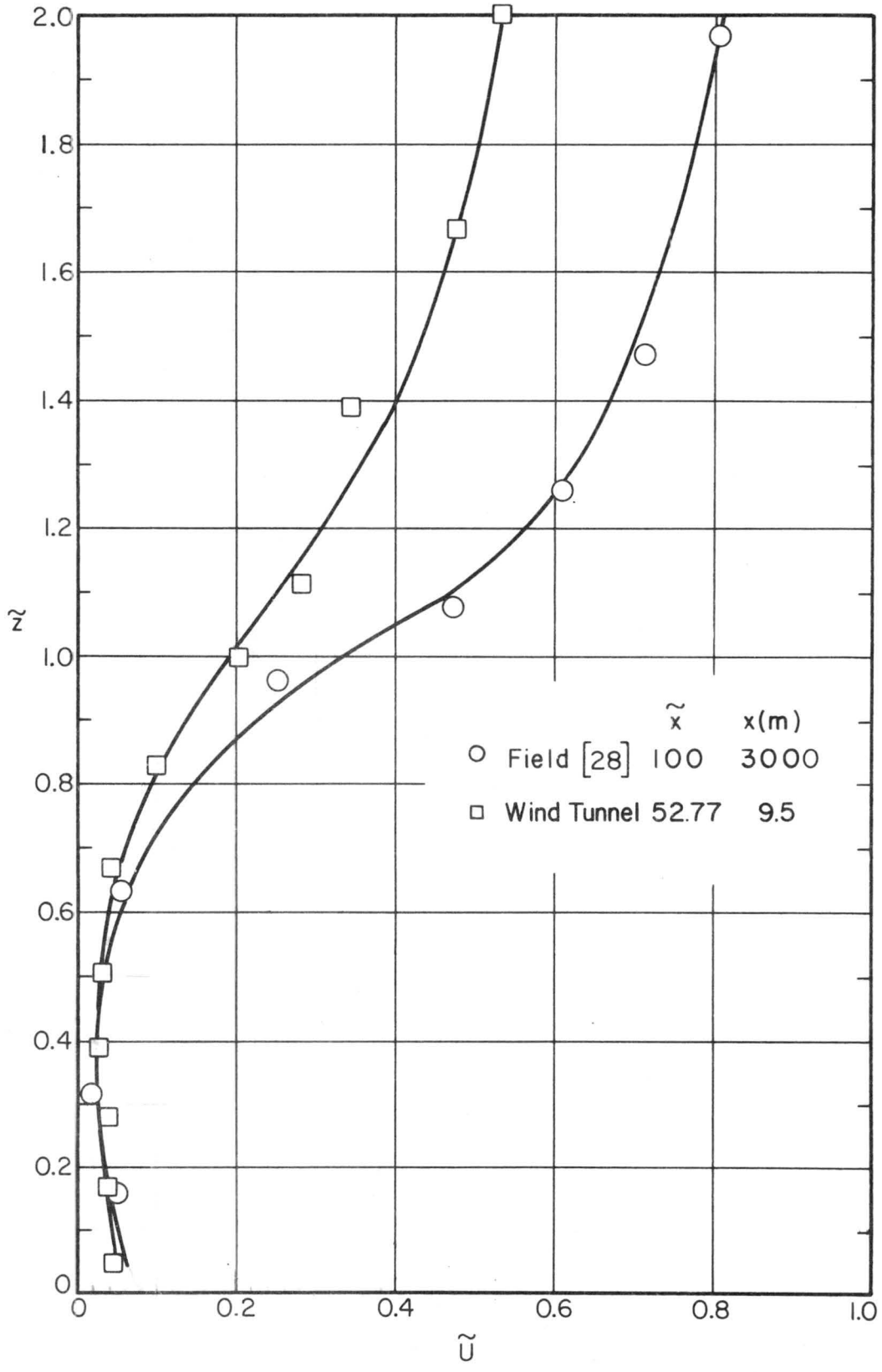

Fig. 4.18 Wind Tunnel and Full-scale Forest Mean Velocity Variation with Height within the Fully Developed Flow Region.

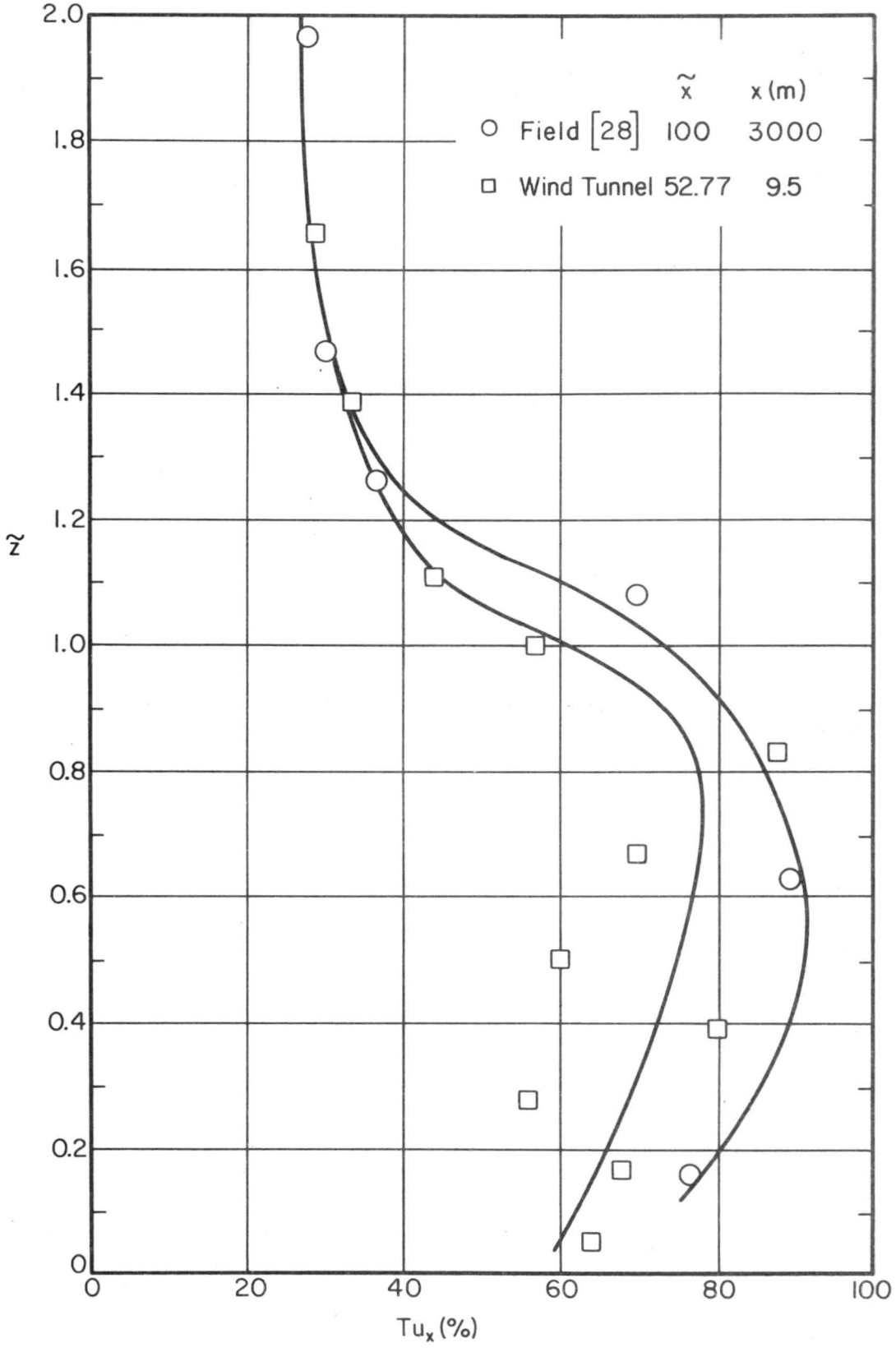

Fig. 4.19 Wind Tunnel and Full-scale Forest Longitudinal Turbulence Intensity Variation with Height within the Fully Developed Flow Region.

APPENDIX A

Mean velocity and longitudinal turbulence intensity

The results for the mean velocity and longitudinal turbulence intensity along the canopy center line, i.e., along the x-axis, are summarized in Table 1. In this table the dimensionless coordinates are defined by Eq. (4.1), the dimenionless mean velocity by Eq. (4.2) and the longitudinal turbulence intensity by Eq. (4.7). Note that $u' = u_{rms}(z)$.

A schematic diagram of the experimental arrangement is shown in Fig. 2.2. The results summarized in this table are displayed in Figs. 4.1 to 4.3 and 4.13 to 4.15, respectively.

TABLE 1

MEAN VELOCITY AND TURBULENCE INTENSITY

X(m) $\tilde{X}$		-1.00 -5.55			0 0			1.00 5.55			2.00 11.11			3.00 16.66		
Z (cm)	$\tilde{Z}$	U (m/s)	$\tilde{U}$	u'/U	U (m/s)	$\tilde{U}$	u'/U	U (m/s)	$\tilde{U}$	u'/U	U (m/s)	$\tilde{U}$	u'/U	U (m/s)	$\tilde{U}$	u'/U
1.0	0.06	3.42	0.570	0.139	2.02	0.337	0.214	1.37	0.228	0.253	0.58	0.097	0.345	0.50	0.083	0.543
3.0	0.17	3.72	0.620	0.139	2.62	0.437	0.197	1.32	0.220	0.330	0.40	0.067	0.434	0.36	0.060	0.598
5.0	0.28	3.92	0.653	0.130	2.79	0.465	0.192	0.59	0.098	0.655	0.36	0.060	0.580	0.30	0.050	0.658
7.0	0.39	4.20	0.700	0.120	2.96	0.493	0.178	0.36	0.060	0.673	0.27	0.045	0.723	0.23	0.038	0.740
9.0	0.50	4.33	0.722	0.119	3.10	0.517	0.158	0.30	0.050	0.560	0.31	0.052	0.715	0.29	0.048	0.738
12.0	0.67	4.45	0.742	0.113	3.17	0.528	0.146	0.30	0.050	0.550	0.48	0.080	0.634	0.42	0.070	0.843
15.0	0.84	4.58	0.763	0.107	3.31	0.552	0.129	0.30	0.050	0.810	0.64	0.107	0.727	0.48	0.080	0.966
17.0	0.95	4.62	0.770	0.106	3.50	0.583	0.127	0.72	0.120	0.578						
18.0	1.00	4.80	0.800	0.099	3.57	0.595	0.116	0.92	0.153	0.568	0.90	0.150	0.676	1.21	0.202	0.668
20.0	1.11	4.80	0.800	0.099	3.88	0.647	0.108	1.00	0.183	0.491	1.42	0.237	0.550	1.23	0.205	0.539
25.0	1.39	4.88	0.813	0.098	4.16	0.693	0.105	2.02	0.337	0.377	1.72	0.287	0.487	1.72	0.287	0.456
30.0	1.67	5.06	0.843	0.092	4.62	0.770	0.096	3.42	0.570	0.217	2.19	0.365	0.404	1.96	0.327	0.437
35.0	1.94	5.06	0.843	0.088	4.71	0.785	0.091	4.16	0.693	0.164	2.69	0.448	0.368	2.59	0.432	0.374
40.0	2.22	5.24	0.873	0.082	4.88	0.813	0.081	4.67	0.778	0.096	3.17	0.528	0.310	3.13	0.522	0.278
45.0	2.50	5.34	0.890	0.068	5.02	0.836	0.074	5.06	0.843	0.076	4.28	0.713	0.193	3.92	0.653	0.231
50.0	2.78	5.66	0.943	0.057	5.15	0.858	0.071	5.15	0.858	0.076	4.97	0.828	0.127	4.37	0.728	0.192
55.0	3.05	5.71	0.952	0.048	5.43	0.905	0.057	5.34	0.890	0.070	5.38	0.897	0.105	4.80	0.800	0.152
60.0	3.33	5.71	0.952	0.035	5.52	0.920	0.041	5.34	0.890	0.069	5.57	0.928	0.085	4.88	0.813	0.114

TABLE 1 (Cont'd)

MEAN VELOCITY AND TURBULENCE INTENSITY

X(m) $\tilde{X}$		5.00 27.77			7.00 38.88			9.50 52.77			11.00 61.11			12.00 66.66		
Z (cm)	$\tilde{Z}$	U (m/s)	$\tilde{U}$	u'/U	U (m/s)	$\tilde{U}$	u'/U	U (m/s)	$\tilde{U}$	u'/U	U (m/s)	$\tilde{U}$	u'/U	U (m/s)	$\tilde{U}$	u'/U
1.0	0.06	0.14	0.023	0.759	0.19	0.032	0.780	0.28	0.047	0.640	0.50	0.083	0.431	0.50	0.083	0.810
3.0	0.17	0.21	0.035	0.575	0.24	0.040	0.677	0.29	0.048	0.678	0.53	0.088	0.472	0.92	0.153	0.657
5.0	0.28	0.17	0.028	0.730	0.25	0.042	0.625	0.25	0.042	0.555	0.42	0.070	0.559	1.32	0.220	0.417
7.0	0.39	0.24	0.040	0.579	0.19	0.032	0.710	0.15	0.025	0.795	0.40	0.067	0.545	1.39	0.232	0.489
9.0	0.50	0.26	0.043	0.615	0.18	0.030	0.795	0.18	0.030	0.600	0.25	0.042	0.752	1.42	0.237	0.485
12.0	0.67	0.38	0.063	0.716	0.30	0.050	0.723	0.28	0.047	0.697	0.37	0.062	0.710	1.66	0.277	0.450
15.0	0.84	0.81	0.135	0.761	0.44	0.073	0.828	0.58	0.097	0.876	0.88	0.147	0.688	1.93	0.322	0.400
18.0	1.00	1.44	0.240	0.562	1.02	0.170	0.655	1.23	0.205	0.572	1.93	0.322	0.513	1.96	0.327	0.412
20.0	1.11	1.61	0.268	0.487	1.44	0.240	0.498	1.72	0.287	0.441	2.07	0.345	0.402	2.02	0.337	0.407
25.0	1.39	2.25	0.375	0.374	1.99	0.332	0.350	2.07	0.345	0.335	2.72	0.453	0.307	2.76	0.460	0.328
30.0	1.67	2.40	0.400	0.313	2.40	0.400	0.289	2.86	0.477	0.289	2.92	0.487	0.241	2.92	0.487	0.285
35.0	1.94	2.82	0.470	0.267	3.20	0.533	0.264	3.03	0.505	0.281	3.39	0.565	0.215	3.24	0.540	0.218
40.0	2.22	2.99	0.498	0.260	3.35	0.558	0.236	3.13	0.522	0.244	3.61	0.602	0.218	3.39	0.565	0.214
45.0	2.50	3.35	0.558	0.237	3.42	0.570	0.212	3.76	0.627	0.204	3.96	0.660	0.180	3.76	0.627	0.193
50.0	2.78	3.72	0.620	0.216	3.80	0.633	0.178	4.00	0.667	0.184	4.33	0.722	0.173	3.84	0.640	0.173
55.0	3.05	3.80	0.633	0.208	4.08	0.680	0.172	4.20	0.700	0.165	4.75	0.792	0.162	4.04	0.673	0.148
60.0	3.33	4.08	0.680	0.182	4.20	0.700	0.170	4.37	0.728	0.162	4.58	0.763	0.150	4.28	0.713	0.135

DOCUMENT CONTROL DATA - R&D

(Security classification of title, body of abstract and indexing annotation must be entered when the overall report is classified)

1. ORIGINATING ACTIVITY *(Corporate author)*
Colorado State University
Foothills Campus
Fort Collins, Colorado 80521

2a. REPORT SECURITY CLASSIFICATION
Unclassified

2b. GROUP

3. REPORT TITLE

"FLOW FIELD WITHIN AND ABOVE A FOREST CANOPY"

4. DESCRIPTIVE NOTES *(Type of report and inclusive dates)*

TECHNICAL REPORT

5. AUTHOR(S) *(Last name, first name, initial)*

Sadeh, W. Z., Cermak, J. E. and Kawatani, T.

6. REPORT DATE
July 1969

7a. TOTAL NO. OF PAGES
67

7b. NO. OF REFS
33

8a. CONTRACT OR GRANT NO.
DAAB07-68-C-0423 (June 1, 1968)

b. PROJECT NO.
2273

c.

d.

9a. ORIGINATOR'S REPORT NUMBER(S)
CER69-70WZS-JEC-TK-6

9b. OTHER REPORT NO(S) *(Any other numbers that may be assigned this report)*

10. AVAILABILITY/LIMITATION NOTICES
Distribution of this report is unlimited

11. SUPPLEMENTARY NOTES

12. SPONSORING MILITARY ACTIVITY
U. S. Army Materiel Command

13. ABSTRACT

The velocity and longitudinal turbulence intentsity distributions inside and above a forest canopy along its center line were investigated. For this purpose a model forest canopy was used in a meteorological wind tunnel.

The results indicate that the flow may be divided into an entrance and fully developed region followed by a short adjustment distance close to canopy end. The entrance region has a decisive effect on the flow characteristics through the canopy. The velocity and turbulence inside the canopy are strongly affected by its structure. A similar qualitative variation for both velocity and turbulence was found in and above the canopy. Its influence stretches over more than 4 roughness heights above it. Generally, the results are in relatively reasonable agreement with field measurements.

Investigation of the modified logarithmic law for describing the velocity profile above the canopy revealed that both flow parameters, i.e., friction velocity and roughness length, are not local constants. On the contrary, they vary drastically with height. It is suspected that this is due to the fact the assumption of constant shear stress throughout the boundary layer or significant portions of it is not satisfied.

DD FORM 1 JAN 64 1473

14. KEY WORDS	LINK A		LINK B		LINK C	
	ROLE	WT	ROLE	WT	ROLE	WT
Simulation Atmospheric Modeling Wind Tunnel Forest Canopies Forest Meteorology Turbulence Fluid Mechanics						

INSTRUCTIONS

1. ORIGINATING ACTIVITY: Enter the name and address of the contractor, subcontractor, grantee, Department of Defense activity or other organization *(corporate author)* issuing the report.

2*a*. REPORT SECURITY CLASSIFICATION: Enter the overall security classification of the report. Indicate whether "Restricted Data" is included. Marking is to be in accordance with appropriate security regulations.

2*b*. GROUP: Automatic downgrading is specified in DoD Directive 5200.10 and Armed Forces Industrial Manual. Enter the group number. Also, when applicable, show that optional markings have been used for Group 3 and Group 4 as authorized.

3. REPORT TITLE: Enter the complete report title in all capital letters. Titles in all cases should be unclassified. If a meaningful title cannot be selected without classification, show title classification in all capitals in parenthesis immediately following the title.

4. DESCRIPTIVE NOTES: If appropriate, enter the type of report, e.g., interim, progress, summary, annual, or final. Give the inclusive dates when a specific reporting period is covered.

5. AUTHOR(S): Enter the name(s) of author(s) as shown on or in the report. Enter last name, first name, middle initial. If military, show rank and branch of service. The name of the principal author is an absolute minimum requirement.

6. REPORT DATE: Enter the date of the report as day, month, year; or month, year. If more than one date appears on the report, use date of publication.

7*a*. TOTAL NUMBER OF PAGES: The total page count should follow normal pagination procedures, i.e., enter the number of pages containing information.

7*b*. NUMBER OF REFERENCES: Enter the total number of references cited in the report.

8*a*. CONTRACT OR GRANT NUMBER: If appropriate, enter the applicable number of the contract or grant under which the report was written.

8*b*, 8*c*, & 8*d*. PROJECT NUMBER: Enter the appropriate military department identification, such as project number, subproject number, system numbers, task number, etc.

9*a*. ORIGINATOR'S REPORT NUMBER(S): Enter the official report number by which the document will be identified and controlled by the originating activity. This number must be unique to this report.

9*b*. OTHER REPORT NUMBER(S): If the report has been assigned any other report numbers *(either by the originator or by the sponsor)*, also enter this number(s).

10. AVAILABILITY/LIMITATION NOTICES: Enter any limitations on further dissemination of the report, other than those imposed by security classification, using standard statements such as:

(1) "Qualified requesters may obtain copies of this report from DDC."

(2) "Foreign announcement and dissemination of this report by DDC is not authorized."

(3) "U. S. Government agencies may obtain copies of this report directly from DDC. Other qualified DDC users shall request through _____."

(4) "U. S. military agencies may obtain copies of this report directly from DDC. Other qualified users shall request through _____."

(5) "All distribution of this report is controlled. Qualified DDC users shall request through _____."

If the report has been furnished to the Office of Technical Services, Department of Commerce, for sale to the public, indicate this fact and enter the price, if known.

11. SUPPLEMENTARY NOTES: Use for additional explanatory notes.

12. SPONSORING MILITARY ACTIVITY: Enter the name of the departmental project office or laboratory sponsoring *(paying for)* the research and development. Include address.

13. ABSTRACT: Enter an abstract giving a brief and factual summary of the document indicative of the report, even though it may also appear elsewhere in the body of the technical report. If additional space is required, a continuation sheet shall be attached.

It is highly desirable that the abstract of classified reports be unclassified. Each paragraph of the abstract shall end with an indication of the military security classification of the information in the paragraph, represented as *(TS)*, *(S)*, *(C)*, *or (U)*.

There is no limitation on the length of the abstract. However, the suggested length is from 150 to 225 words.

14. KEY WORDS: Key words are technically meaningful terms or short phrases that characterize a report and may be used as index entries for cataloging the report. Key words must be selected so that no security classification is required. Identifiers, such as equipment model designation, trade name, military project code name, geographic location, may be used as key words but will be followed by an indication of technical context. The assignment of links, rules, and weights is optional.

MINIMUM BASIC DISTRIBUTION LIST FOR USAMC SCIENTIFIC AND TECHNICAL REPORTS IN METEOROLOGY AND ATMOSPHERIC SCIENCES

Commanding General (1)
U. S. Army Materiel Command
Attn: AMCRD-RV-A
Washington, D. C. 20315

Commanding General (1)
U. S. Army Electronics Command
Attn: AMSEL-EW
Fort Monmouth, New Jersey 07703

Commanding General (1)
U. S. Army Test and Evaluation Command
Attn: NBC Directorate
Aberdeen Proving Ground, Maryland 21005

Commanding Officer (1)
U. S. Army Ballistics Research Laboratories
Attn: AMXBR-IA
Aberdeen Proving Ground, Maryland 21005

Chief, Atmospheric Physics Division (2)
Atmospheric Sciences Laboratory
U. S. Army Electronics Command
Fort Monmouth, New Jersey 07703

U. S. Army Munitions Command (1)
Attn: Irving Solomon
Operations Research Group
Edgewood Arsenal, Maryland 21010

Commanding Officer (1)
U. S. Army Dugway Proving Ground
Attn: Meteorology Division
Dugway, Utah 84022

Commanding Officer (1)
U. S. Army CDC, CBR Agency
Attn: Mr. N. W. Bush
Fort McClellan, Alabama 36205

Commanding General (1)
U. S. Army Test and Evaluation Command
Attn: AMSTE-EL
Aberdeen Proving Ground, Maryland 21005

Assistant Chief of Staff for Force Development (1)
CBR Nuclear Operations Directorate
Department of the Army
Washington, D. C. 20310

Director (1)
Atmospheric Sciences Programs
National Sciences Foundation
Washington, D. C. 20550

Assistant Secretary of Defense (1)
Research and Engineering
Attn: Technical Library
Washington, D. C. 20301

R. A. Taft Sanitary Engineering Center (1)
Public Health Service
4676 Columbia Parkway
Cincinnati, Ohio

Dr. Hans A. Panofsky (1)
Department of Meteorology
The Pennsylvania State University
University Park, Pennsylvania

Commanding General (1)
U. S. Continental Army Command
Attn: Reconnaissance Branch ODCS for Intelligence
Fort Monroe, Virginia 23351

Commander (1)
Air Force Cambridge Research Laboratories
Attn: CRZW
1065 Main Street
Waltham, Massachusetts

President (1)
U. S. Army Artillery Board
Fort Sill, Oklahoma 73504

National Center for Atmospheric Research (1)
Attn: Library
Boulder, Colorado

Dr. J. E. Cermak, Head (15)
Fluid Mechanics Program
Colorado State University
Fort Collins, Colorado 80521

Author (1)

Chief of Research and Development (1)
Department of the Army
Attn: CRD/M
Washington, D. C. 20310

Commanding General (1)
U. S. Army Missile Command
Attn: AMSMI-RRA
Redstone Arsenal, Alabama 35809

Commanding General (1)
U. S. Army Natick Laboratories
Attn: Earth Sciences Division
Natick, Massachusetts 01762

Director, U. S. Army Engineer (1)
Waterways Experiment Station
Attn: WES-FV
Vicksburg, Mississippi 39181

Chief, Atmospheric Sciences Research Division (5)
Atmospheric Sciences Laboratory
U. S. Army Electronics Command
Fort Huachuca, Arizona 85613

Commanding Officer (1)
U. S. Army Frankford Arsenal
Attn: SMUFA-1140
Philadelphia, Pennsylvania 19137

Commandant
U. S. Army Artillery and Missile School
Attn: Target Acquisition Department
Fort Sill, Oklahoma 73504

Commanding General (1)
U. S. Army Test and Evaluation Command
Attn: AMSTE-BAF
Aberdeen Proving Ground, Maryland 21005

Office of Chief Communications - Electronics (1)
Department of the Army
Attn: Electronics Systems Directorate
Washington, D. C. 20315

Chief of Naval Operations (1)
Department of the Navy
Attn: Code 427
Washington, D. C. 20350

Director (1)
Bureau of Research and Development
Federal Aviation Agency
Washington, D. C. 20553

Director of Meteorological Systems (1)
Office of Applications (FM)
National Aeronautics and Space Administration
Washington, D. C. 20546

Director (1)
Atmospheric Physics and Chemistry Laboratory
Environmental Science Services Administration
Boulder, Colorado

Andrew Morse (1)
Army Aeronautical Activity
Ames Research Center
Moffett Field, California 94035

Commanding Officer (2)
U. S. Army Cold Regions Research and Engineering Laboratories
Attn: Environmental Research Branch
Hanover, New Hampshire 03755

Mr. Ned L. Kragness (1)
U. S. Army Aviation Materiel Command
SMOSM-E
12th and Spruce Streets
Saint Louis, Missouri 63166

Commanding Officer, U. S. Army (1)
Artillery Combat Development Agency
Fort Sill, Oklahoma 73504

Commander, USAR Air Weather Service (MATS) (1)
Attn: AWSSS/TIPD
Scott Air Force Base, Illinois

Dr. John Bogusky (1)
7310 Cedardale Drive
Alexandria, Virginia 22308

Commanding General (1)
U. S. Army Combat Development Command
Attn: CDCMR-E
Fort Belvoir, Virginia 22060

Commanding General (1)
U. S. Army Munitions Command
Attn: AMSMU-RE-R
Dover, New Jersey 07801

Commanding Officer (1)
U. S. Army Ballistics Research Laboratories
Attn: AMXBR-B
Aberdeen Proving Ground, Maryland 21005

Director (2)
Atmospheric Sciences Laboratory
U. S. Army Electronics Command
White Sands Missile Range, New Mexico 88002

Chief, Atmospheric Sciences Office (2)
Atmospheric Sciences Laboratory
U. S. Army Electronics Command
White Sands Missile Range, New Mexico 88002

Commanding Officer (1)
U. S. Army Picatinny Arsenal
Attn: SMUPA-TV-3
Dover, New Jersey 07801

Commanding Officer (1)
U. S. Army Communications - Electronics Combat Development Agency
Fort Monmouth, New Jersey 07703

Commanding General (1)
Deseret Test Center
Attn: Design and Analysis Division
Fort Douglas, Utah 84113

Commandant (1)
U. S. Army CBR School Micrometeorological Section
Fort McClellan, Alabama 36205

Assistant Chief of Staff for Intelligence (1)
Department of the Army
Attn: ACSI-DERSI
Washington, D. C. 20310

Commanding Officer (1)
U. S. Naval Weather Research Facility
U. S. Naval Air Station, Building R-48
Norfolk, Virginia 23511

Chief, Fallout Studies Branch (1)
Division of Biology and Medicine
Atomic Energy Commission
Washington, D. C. 20545

Director (1)
U. S. Weather Bureau
Attn: Librarian
Washington, D. C. 20235

Dr. Albert Miller (1)
Department of Meteorology
San Jose State College
San Jose, California 95114

Mrs. Francis L. Wheedon (1)
Army Research Office
3045 Columbia Pike
Arlington, Virginia 22201

Commander (1)
Air Force Cambridge Research Laboratories
Attn: CRXL
L. G. Hanscom Field
Bedford, Massachusetts

Harry Moses, Asso. Meteorologist (1)
Radiological Physics Division
Argonne National Laboratory
9700 S. Cass Avenue
Argonne, Illinois 60440

Defense Documentation Center (20)
Cameron Station
Alexandria, Virginia 22314

Office of U. S. Naval Weather Service (1)
U. S. Naval Air Station
Washington, D. C. 20390

Dr. Gerald Gill (1)
University of Michigan
Ann Arbor, Michigan 48103